A sustainable strategy for generating highly stable human skin equivalents based on fish collagen

Shi Hua Tan[1], Shaoqiong Liu[2], Swee Hin Teoh[3], Carine Bonnard[1,4], David Leavesley[4], Kun Liang[1,4*].

[1]A*STAR Skin Research Labs (A*SRL), Agency for Science, Technology and Research (A*STAR), Singapore

[2]School of Chemical and Biomedical Engineering, Nanyang Technological University, Singapore

[3]College of Materials Science and Engineering, Hunan University, People's Republic of China

[4]Skin Research Institute of Singapore (SRIS), Singapore

*Correspondence: Kun Liang

Email: kun_liang@asrl.a-star.edu.sg

Keywords:

Human skin equivalent, hydrogel scaffold, 3D skin model

Abbreviations:

ATR-FTIR	Attenuated Total Reflectance-Fourier Transform Infrared Spectroscopy
BC	Bovine collagen
CD	Circular dichroism
DSC	Differential scanning calorimeter
FBC	Fortified bovine collagen
FC	Fish collagen
FFC	Fortified fish collagen
H&E	Hematoxylin and eosin
HDF(s)	Human dermal fibroblast(s)
HEK(s)	Human epidermal keratinocyte(s)
HSE(s)	Human skin equivalent(s)
IHC	Immunohistochemistry
MTT	Thiazolyl blue tetrazolium bromide
SDS-PAGE	Sodium dodecyl sulphate−polyacrylamide gel electrophoresis
SEM	Scanning electron microscopy
Td	Denaturation temperature
TEER	Transepithelial electrical resistance

Abstract

Tissue engineered skin equivalents are increasingly recognized as potential alternatives to traditional skin models such as human *ex vivo* skin or animal skin models. However, most of the currently investigated human skin equivalents (HSEs) are constructed using mammalian collagen which can be expensive and difficult to extract. Fish skin is a waste product produced by fish processing industries and identified as a cost-efficient and sustainable source of type I collagen. In this work, we describe a method for generating highly stable HSEs based on fibrin fortified tilapia fish collagen. The fortified fish collagen (FFC) formulation is optimized to enable reproducible fabrication of full-thickness HSEs that undergo limited contraction, facilitating the incorporation of human donor-derived skin cells and formation of biomimetic dermal and epidermal layers. The morphology and barrier function of the FFC HSEs are compared with a commercial skin model and validated with immunohistochemical staining and transepithelial electrical resistance testing. Finally, the potential of a high throughput screening platform with FFC HSE is explored by scaling down its fabrication to 96-well format.

1. Introduction

Living human skin models are critical tools in advancing our understanding of basic skin physiology, investigating disease pathology, and performing compound evaluations within the pharmaceutical and cosmetic industries. Traditionally, assessment of different substances on our cutaneous barrier has been performed on freshly excised human skin or using animals such as rodents, rabbits and pigs as *ex vivo* or *in vivo* skin models [1–3]. However, since the implementation of EU Directive 2010/63/EU, which completely banned animal testing for cosmeceutical products from 2013, alternative methods are required to replace the use of animals in cosmeceutical product testing [4,5]. In addition, the logistical challenges associated with obtaining *ex vivo* human skin for testing product safety and efficacy has further driven the development of *in vitro* tissue engineered human skin equivalents (HSEs), replacing these traditional testing regimens.

To successfully recreate the structure and function of human skin, many investigators within the field have sought to fabricate hydrogel-based HSEs using type I collagen, since collagen is the main component of the dermal extracellular matrix, and provides both structural and cell regulatory functions [6,7]. While collagen, its derivatives and combinations with other natural, synthetic or cross-linking materials, have been efficaciously utilized in generating the dermal equivalent of HSEs [8–15], the type I collagen used to construct these models are often derived from mammalian sources, requiring costly and/or laborious production [16–18].

Recently, marine organisms ranging from invertebrates, such as jellyfish and sponges, to vertebrates such as bony fishes and cartilaginous sharks, have attracted attention as alternative sources of collagen [19–21]. Notably, underutilized by-products of the fishing industry such as fish skin contain mostly type I collagen constituting around 70% of its dry weight [22–24]. The

collagen derived from fish skin maintains similar molecular structure and bioactivity to mammalian collagen [6,25,26], carries less risk for zoonotic disease transmission, is less immunogenic due to absence of antigenic mammalian proteins and can be applied without religious concerns [16,18,27,28].

Nonetheless, the use of fish skin collagen presents some challenges which can limit its applications in tissue engineering. Generally, fish collagen contain lesser imino acid content (hydroxyproline and proline), leading to lowered denaturation temperatures of <30 °C compared to terrestrial mammalian collagens that denature between 39-40 °C [29,30]. In addition, the low hydroxyproline content of fish collagen can affect its mechanical stability, restricting the practical use of fish collagen products under usual cell culture temperatures, or within the human body [31]. There are, however, exceptions. Warm-water fishes such as the Nile tilapia (*Oreochromis niloticus*) have been reported to have a higher degree of proline hydroxylation leading to increased denaturation temperatures of around 30-36 °C [32–35]. Moreover, tilapia is the second-most farmed fish globally after carp, contributing a large volume of discarded fish waste and by-products that further contribute to tilapia skin as an eco-friendly source of mammalian collagen substitute [36]. To exploit tilapia skin-derived collagen for different tissue engineering applications, several investigators have also explored physical and chemical cross-linking or blending with other bioactive materials to improve the mechanical and thermal properties of tilapia collagen [37,38]. These tilapia skin collagen scaffolds have been utilized for bone tissue engineering [39,40], cartilage repair [41] as well as wound healing purposes [37,42].

In this study, we have investigated the application of tilapia skin collagen for *in vitro* reconstruction of human skin tissue. Collagen was extracted and purified from tilapia skin

using acid solubilization and physicochemical properties of the resulting material was systematically characterized. To improve the mechanical properties of fish collagen (FC) to support the attachment and growth of human skin-derived fibroblasts, an optimized amount of fibrin was blended with FC to obtain fortified fish collagen (FFC). Fibrinogen, and its insoluble polymer, fibrin, is commonly added to collagen-based formulations to mediate cell-induced contraction of collagen matrices [43–48]. Compared to physical, or chemical cross-linking strategies, blending collagen with a natural biopolymer such as fibrin may exhibit less cytotoxicity. The FFC constructs were observed to resist fibroblast-mediated contraction and demonstrated good cell compatibility. When used to construct dermal equivalents, FFC supported the growth of both fibroblasts and keratinocytes, facilitating the formation of bilayered full-thickness HSEs. FFC HSEs maintained optimal structural stability over the entire duration of culture *in vitro* when compared to FC HSEs and HSEs constructed with bovine collagen (BC) or fortified bovine collagen (FBC). Finally, the morphology and function of FFC and FBC HSEs were compared to a commercially validated full-thickness skin equivalent (EpiDermFT™, MatTek), as well as to native human skin. FFC HSEs displayed structural similarity to native human skin and exhibited the highest transepithelial electrical resistance (TEER) among all skin models tested. Therefore, valorization of tilapia skin collagen transforms a largely discarded waste product into a cost-effective and sustainable material source for generating viable, authentic HSEs (Figure 1).

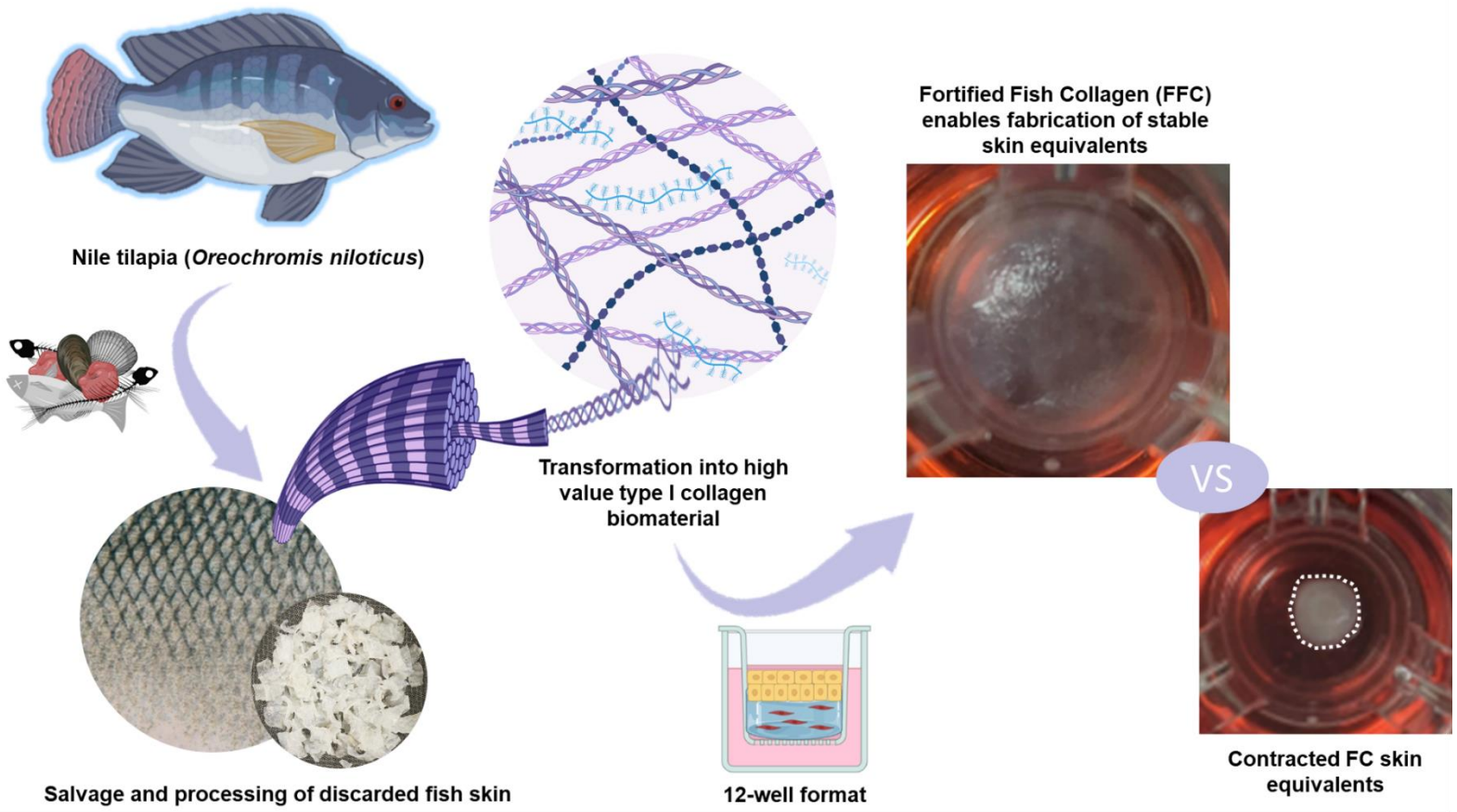

Figure 1. Valorization of tilapia skin collagen transforms a discarded waste product of the fishing industry, into high value type I collagen biomaterial. To support the cultivation of human skin equivalents, the physicochemical properties of tilapia skin collagen were improved through fortification of the extracted fish collagen (FFC), generating an optimized scaffold formulation that resisted the cell-mediated contraction observed in fish collagen alone (FC).

2. Materials and methods

2.1 Materials

Fresh tilapia skin was purchased from Hai Sia Seafood Pte Ltd (Singapore). Acetic acid, butanol, isopropanol, NaOH, NaCl, hydroxyproline assay kit, adenine, hydrocortisone, transferrin, triiodo-L-thyronine, insulin and Thiazolyl Blue Tetrazolium Bromide (MTT) were purchased from Sigma-Aldrich (USA). Biocolor Sircol™ Insoluble Collagen Assay reagents were purchased from Biocolor (UK). Protein standards, reagents, and apparatus for SDS−PAGE were acquired from Bio-Rad (USA). All other cell culture reagents were purchased from Thermo Fisher Scientific (USA), and all other chemicals were of analytical grade and used upon receipt.

2.2 Extraction of tilapia collagen

The tilapia fish collagen extraction was performed according to the method reported in our previous studies, with slight modifications [49]. Briefly, fish skin was de-scaled, washed with distilled water and then soaked in 0.1 M NaOH for 6 hours to remove non-collagenous proteins. Fish skin was then soaked in 10% butyl alcohol for 1 day, to remove attached fats. Thereafter, the skin was transferred to a mixer with 200 volumes of 0.5 M acetic acid and stirred continuously until collagen was solubilized. The resulting crude solution was centrifuged to remove particulate matter, the supernatant collected and NaCl added to precipitate collagens. The collagen precipitates were recovered and re-dissolved in 0.5 M acetic acid. This product was dialyzed against 0.1 M acetic acid for 24 hours followed by dialysis against distilled water for 48 hours. After dialysis, samples were lyophilized, and the dried collagen sponges were stored for future analysis. Yield of extracted collagens were calculated based on the weight ratios of lyophilized collagens and dry weight of the starting material. The purity of the collagen was quantified using the Biocolor Sircol™ Insoluble Collagen Assay.

2.3 Physico-chemical characterization of tilapia collagen

Sodium dodecyl sulphate−polyacrylamide gel electrophoresis (SDS-PAGE) was performed to determine the molecular weight of protein subunits from tilapia collagen preparations, according to the manufacturer's instructions (Bio-Rad). Attenuated Total Reflectance-Fourier Transform Infrared (ATR-FTIR) Spectroscopy of tilapia collagen samples was acquired using a Nicolet™ FTIR spectrophotometer (Thermo Fisher Scientific, USA). The amino acid composition of each collagen sample was analyzed using a Hitachi L-8800 amino acid analyzer (Hitachi High-Technologies Corp, Japan). It is noted that hydroxyproline was quantified using hydroxyproline assay kit based on manufacturer's instruction (Sigma). The thermal stability of the collagen (2.5% (w/v) in 0.05 M acetic acid) was determined by the Q10 Differential Scanning Calorimeter (DSC) (TA Instruments, USA). Denaturation temperature (T_d) was estimated from the endothermic peak of DSC thermogram. Circular dichroism (CD) spectra were recorded using a Chirascan CD spectrometer (Applied Photophysics, UK). Spectra were recorded from 250 nm to 190 nm at 50 nm/minute. The mean ellipticity was calculated using the equation: $[\theta]_\lambda = (M/(N-1)\times\theta_\lambda)/(d \times c)$ [50], where M denotes the molecular weight of collagen, N represents the number of amino acid residues, θ_λ is the ellipticity (degrees) at wave length λ, d is pathlength (cm), c represents the concentration (g/mL) and $[\theta]_\lambda$ denotes mean residue ellipticity with a unit of deg cm^2 $dmol^{-1}$. R_{pn} was calculated as ellipticity ratio of positive peak over negative peak.

2.4 Cell culture

Human dermal fibroblasts (HDFs) and epidermal keratinocytes (HEKs) were provided by the Asian Skin Biobank, Skin Research Institute of Singapore, A*STAR (IRB 2020-209). HDFs were cultured in DMEM supplemented with 10% FBS, 1% penicillin-streptomycin (fibroblast

medium) and used up to passage 6. HEKs were cultured in the presence of irradiated 3T3-J2 embryonic mouse fibroblasts in FAD medium (DMEM:Ham's F12 3:1, supplemented with 10% FBS, 1% penicillin-streptomycin, $1.8x10^{-4}$ M adenine, 0.4 µg/mL hydrocortisone, 5 µg/mL transferrin, $2x10^{-9}$ M triiodo-L-thyronine, $1x10^{-10}$ M cholera toxin, 5 µg/mL insulin and 10 ng/mL epidermal growth factor) [51–53] and used up to passage 3. Medium was changed every 2-3 days until cells reached around 80% confluence where they were trypsinized with 0.05% Trypsin-EDTA for downstream applications or continued culture.

2.5 Optimization of collagen-fibrin formulation

Lyophilized fish collagen was resolubilized in 20 mM acetic acid at a concentration of 5 mg/mL and kept at 4 °C. To prepare the collagen-based scaffolds, ice-cold collagen solution (final concentration 3 mg/mL) was mixed with 10x MEM (10% of total volume), $NaHCO_3$ (final concentration 0.15% w/v) and neutralized with 1 M NaOH. For collagen scaffolds with fibrin, fibrinogen (#F3879, Sigma-Aldrich) was mixed in varying amounts to reach final concentrations of 0 mg/mL – 5 mg/mL. Once the gels were solidified, medium with 5 U/mL thrombin (#T6884, Sigma-Aldrich) was added to the wells to induce fibrin polymerization in the hydrogel scaffolds. Fish collagen scaffolds without fibrin were denoted as F3 while scaffolds with fibrin (Fbn) were denoted as F3-Fbn*X*, where *X* refers to the concentration of fibrin.

To investigate the contraction effect of the fish collagen with varying fibrin concentrations, HDFs at $1x10^5$ cells/mL were evenly dispersed within the mixture, pipetted into 96-well plates and placed into a 37 °C incubator for gel solidification. Once the gel was solidified, fibroblast medium with thrombin was added to the wells. After 24 hours, fresh medium without thrombin was replaced in the wells with media change every 3-4 days. Fibroblast-encapsulated hydrogel

scaffolds were cultured for 14 days. Images were acquired using the EVOS® FL Imaging System (Thermo Fisher Scientific, USA), at different timepoints to track the contraction of scaffolds as they detached from the wall of the wells.

To investigate the attachment of keratinocytes on fish collagen with varying fibrin concentrations, HEKs were resuspended in FAD medium with thrombin and seeded at 0.625 x 10^5 cells/cm^2 on solidified acellular gels. After 24 hours, fresh medium without thrombin was replaced in the wells with media change every 2 days. Keratinocytes seeded on hydrogel scaffolds were cultured for 4 days to investigate their attachment and proliferation on the scaffold surface. At Day 2 and Day 4 post seeding, scaffold surfaces were gently washed with Dulbecco's phosphate buffered saline (DPBS) to remove unattached keratinocytes. Visualization of keratinocyte attachment on the scaffold surfaces was performed by staining with 0.5 mg/mL Thiazolyl Blue Tetrazolium Bromide (MTT) and distribution of surviving keratinocytes was observed through formation of insoluble purple formazan.

2.6 Rheological analysis

The rheological properties such as gelation time, storage modulus G' (G prime, in Pa) and loss modulus G" (G double prime, in Pa) were investigated using an Anton Paar MCR-102 rheometer (Anton Paar GmbH, Graz, Austria). Three mg/mL of acellular fish collagen hydrogels without fibrin (F3) and with fibrin (F3-Fbn0.5) were prepared as described above. To compare fish skin collagen with mammalian collagen, commercially sourced bovine collagen (#A1064401, Thermo Fisher Scientific) was prepared in similar hydrogel format (B3) for investigation. Briefly, 300 µL of hydrogel samples were prepared fresh before each test using chilled pipette tips and vortexed to ensure homogeneity. The samples were kept on ice before loading onto a 35 mm diameter, 1° measuring cone with a mineral oil solvent trap used

to prevent any evaporation. Prior to loading, the rheometer bed was set at 5 °C. The temperature was first kept at 5 °C for 2 minutes, ramped from 5 °C to 37 °C for 15 minutes and held at 37 °C for 60 minutes.

2.7 Cell compatibility of FFC and FBC

The final optimized collagen-fibrin formulation used for downstream analysis was 3 mg/mL of fish/bovine collagen + 0.5 mg/mL of fibrin; otherwise referred to as fortified fish collagen (FFC) or fortified bovine collagen (FBC). To investigate the cell compatibility of optimized hydrogel formulations, HDFs at $1x10^5$ cells/mL were encapsulated in either FFC or FBC scaffolds, and their metabolism, proliferation, and viability, assayed after 1, 4, 7, 11 and 14 days post-seeding. Fibroblast metabolism was investigated using the CellTiter-Glo® Luminescent Cell Viability Assay (Promega Corp, USA) and the assay was performed according to manufacturer's protocol. To investigate fibroblast proliferation, scaffolds were digested with Gibco™ Collagenase Type I (Thermo Fisher Scientific, USA) to release cells which were then manually counted using a hemocytometer. Fibroblast viability was investigated using LIVE/DEAD™ Viability/Cytotoxicity Kit (Thermo Fisher Scientific, USA) and performed according to manufacturer's protocol.

2.8 Scanning electron microscopy imaging

The surface morphology of acellular FFC and FBC scaffolds were examined using scanning electron microscopy (SEM). The specimens were firstly fixed in 4% paraformaldehyde and 2% glutaraldehyde, and then rinsed in DPBS and freeze-dried. Subsequently, the samples were sputter coated with platinum and visualized using a JSM-6701F scanning electron microscope (JEOL, Japan).

2.9 Fabrication of full-thickness 3D human skin equivalents (HSEs)

The dermal equivalent for HSE assembly was prepared using methods similar to those described above. HDFs were encapsulated in either FFC, or FBC, scaffolds at $0.375x10^5$ cells/mL, pipetted evenly onto 0.4 µm pore polyethylene terephthalate membrane Transwell® supports inserted in 12-well plates (#CLS3460, Corning®) and incubated at 37 °C for 1 hour to polymerise. Once solidified, $0.3\ x10^5$ HEKs resuspended in FAD medium with thrombin was seeded onto the apical dermal surface and the same medium was added to the lower wells of each Transwell® plate. Keratinocytes were allowed to attach and proliferate for 2 days, whereafter the immature skin tissue constructs were transferred to deep-well plates to achieve an air-liquid interface. The HSEs were maintained at air-liquid interface for 14 days using ALI medium (FAD medium without EGF) with medium change every 3-4 days. To fabricate FFC HSEs in 96-well plate format, the same preparation protocol was used except reagents and cells required were scaled down 10 times. Microscale FFC HSEs were grown on 0.4 µm pore size polycarbonate membrane HTS Transwell® 96-well supports (#CLS3381, Corning®). EpiDerm™ Full Thickness human skin models (#EFT-412-7A) were purchased in 12-well format from MatTek Corporation (USA) and cultured according to manufacturer's protocol until maturity. EpiDerm™ Full Thickness human skin models (EpiDermFT™) were used as a validated commercial standard for comparison with FFC and FBC full-thickness HSEs.

2.10 Histological Analysis

To relate histological results of the *in vitro* skin models to native human skin, fresh adult Caucasian male abdomen skin was purchased commercially (Genoskin, France, A*STAR IRB 2019-094) and processed to remove excess adipose tissues and hair. The normal adult human skin (NHS), EpiDermFT™, FFC and FBC full-thickness HSEs were fixed for at least 24 hours in 10% neutral buffered formalin and processed according to standard paraffin wax embedding.

Thin slices, 7 µm thickness, were cut, mounted on glass microscope slides, and processed for staining with hematoxylin and eosin (H&E), and for immunohistochemistry (IHC). For IHC processing, samples were deparaffinized, subject to heat-induced epitope retrieval (samples for Collagen IV required an additional 20 minutes of proteinase K treatment), quenched with 1% H_2O_2 and saturated with 10% goat serum, before a 2-hour incubation with primary antibodies at room temperature. The following primary antibodies were used: Keratin 14 ab181595, Loricrin ab176322, Claudin I ab140349, p63 ab735 (Abcam, Cambridge UK); E-cadherin 610182 (BD Transduction Laboratories, USA); Keratin 10 M7002, Collagen IV M0785, Ki67 M7240 (Agilent-DAKO, USA) and Vimentin NCL-L-VIM-V9 (Leica BioSystems, Germany). Slides were next incubated with DAKO EnVision+ System HRP-Labelled Polymer (Agilent-DAKO, USA) for anti-mouse K4001, or anti-rabbit K4003, followed by DAB+ chromogen substrate K3468 (Agilent-DAKO, USA), and counterstained with hematoxylin. To calculate the proliferation index, the number of Ki67-positive basal cells was divided by the total number of epidermal basal cells x 100%. The number of positively stained Ki67 basal cells were counted at 100x magnification in randomly chosen areas of tissue sections covering minimally 100 basal keratinocytes. Positive Ki67 cells were counted for at least 3 different constructs to determine the average proliferation index of either FFC or FBC HSEs.

2.11 Transepithelial electrical resistance (TEER)

Transepithelial electrical resistance (TEER) was investigated using the EVOM2 epithelial volt/ohm meter and EndOhm-12 chambers (WPI, USA) to determine the barrier integrity of EpiDermFT™ and full-thickness HSEs. Skin constructs were allowed to equilibrate to room temperature for 15 minutes before being gently rinsed 3 times with DPBS to remove residual cell culture medium and transferred to EndOhm-12 chambers filled with DPBS. The upper compartment of Transwells® was filled with DPBS to ensure that the internal and external

fluid height was equal after the electrode cap was inserted in place. To calculate the TEER values, resistance measurements from a blank insert with an acellular dermal equivalent was subtracted from the resistance measurements for HSE samples and multiplied by the surface area (1.12 cm^2).

2.12 Statistics

All data indicate mean ± SD. *, **, *** and **** indicate a statistically significant difference with $p < 0.05$, $p < 0.01$, $p < 0.001$ and $p < 0.0001$ respectively (two-tailed unpaired t-tests or one-way ANOVA with Tukey's Multiple Comparison Test).

3. Results

3.1 Extraction and characterization of tilapia fish collagen

Collagen was extracted from the skin of tilapia using a slight modification of our published acid extraction method [49]. The extraction yield of collagen was 42 ± 1%. Results from Sircol insoluble collagen assay indicated that tilapia collagen preparations had a remarkably high purity of close to 100%. SDS-PAGE characterization of the tilapia collagen preparation showed the presence of α, β and γ subunits, with a ratio of two to one for α1:α2 subunits, which is characteristic for type I collagen (Figure 2A).

The analysis of tilapia collagen amino acid composition showed that the most abundant amino acids in tilapia collagen samples were Glycine (331/1000 residues), Alanine (120/1000 residues), Proline (118/1000 residues) and Hydroxyproline (81/1000 residues) (Figure 2B). The presence of $(Gly\text{-}X\text{-}Y)_n$ repeating motifs in the polypeptide chains facilitates the unique triple helical secondary structure, which in turn increases the stability of the collagen fibrillar structure, where X and Y mostly refers to hydroxyproline and proline (imino acids) [54]. Imino

acids, especially hydroxyproline, are critical contributors to the thermal stability of mature collagens [18,30]. Notably, the extracted tilapia collagen was found to be rich in imino acids (199/1000 residues).

It has been recognized that incorporating marine collagens in biomedical applications is challenging due to their low denaturing temperature (T_d) [30]. Collagens having a higher T_d are therefore preferred, as they exhibit greater thermal stability and functionality in mammalian tissues. DSC analysis indicated that the tilapia collagen preparation exhibited a T_d of 39.4 °C, indicative of thermal stability that is commensurate with mammalian tissues (Figure 2C). To the best of our knowledge, the tilapia collagen preparation reported in this study exhibited a significantly higher T_d than the majority of marine collagen preparations reported in the literature, mainly due to its high imino acid content [55].

The collagen triple helix structure is critical to its biological function. CD spectral analysis of tilapia collagen exhibited a maximum positive peak at 220 nm, an intersection with the X-axis at 214 nm, and a minimum negative peak at 197 nm, indicative of natural type I collagen (Figure 2D). Moreover, the ratio of positive to negative peak intensity value R_{pn}, estimated to be 0.11, indicated that the tilapia collagen preparation retained the innate triple helix structure in aqueous solution at a concentration of 0.125 mg/mL [56].

To further analyze the primary and secondary structures of the tilapia collagen preparation, we performed ATR-FTIR spectral analysis. Characteristic peaks of Amide I, II, III and A, B were observed (Figure 2E). The peaks were associated with amide groups at 1635 cm^{-1} for Amide I, 1550 cm^{-1} for Amide II and 1246 cm^{-1} for Amide III [54], which is consistent with our SDS-

PAGE and CD findings. Collectively, these results indicated that the acid-extracted tilapia collagen retained structural integrity.

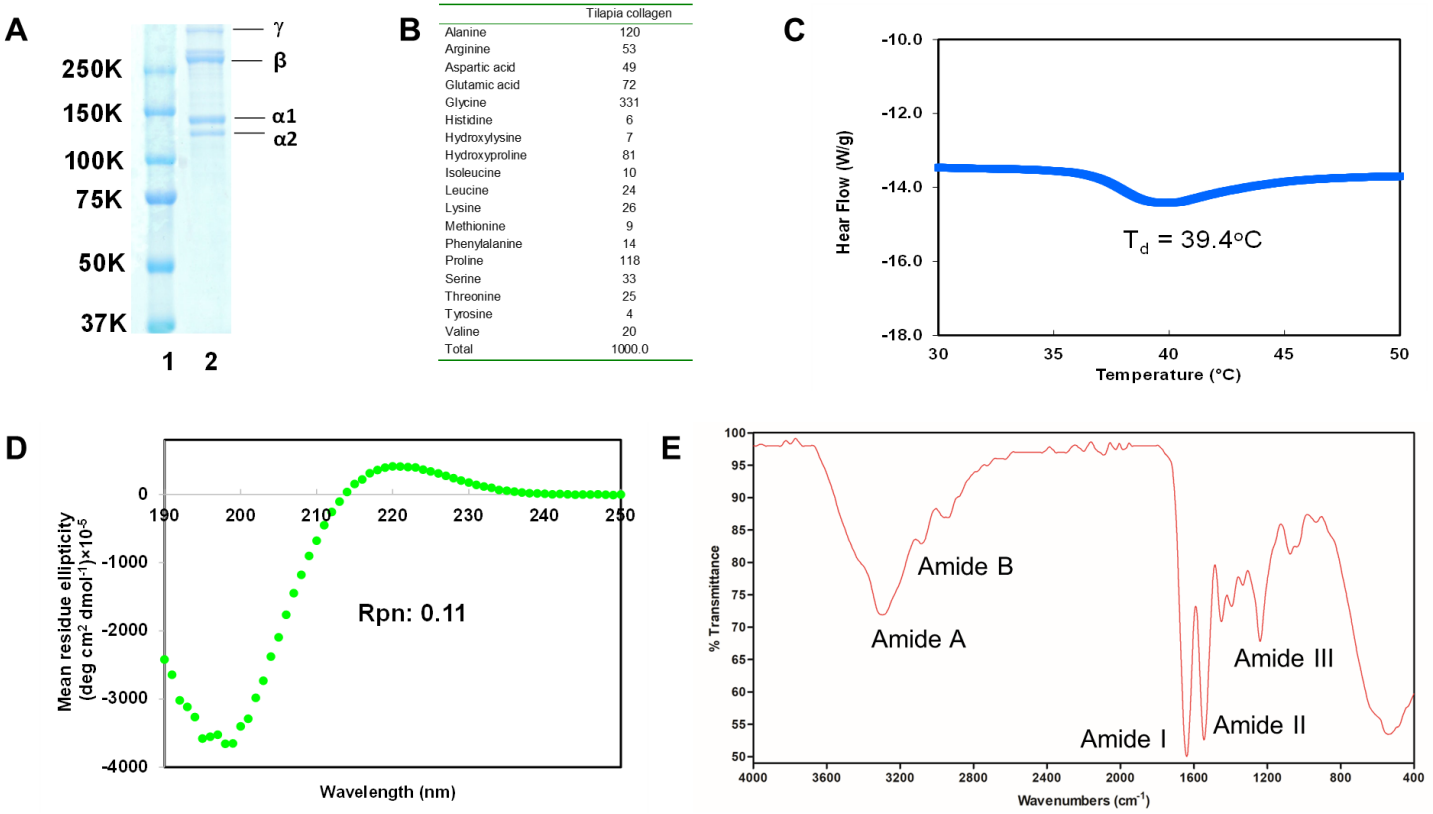

Figure 2. Characterization of tilapia collagen. (A) SDS-PAGE analysis of tilapia collagen (Lane 1 – protein standards ladder; lane 2 – tilapia collagen preparation). (B) Amino acids composition analysis of tilapia collagen preparation (expressed in residues/1000 amino acid residues). (C) DSC thermograms of tilapia collagen preparation. (D) CD Spectra of tilapia collagen preparation (0.125 mg/mL in aqueous solution). (E) ATR-FTIR spectra of tilapia collagen preparation.

3.2 Optimization of fibrin content in fish collagen scaffolds

Contraction is a common phenomenon observed when cells are grown in various collagen scaffolds [57,58]. Dermal fibroblasts generate contractile forces that propagate throughout the collagen scaffold, resulting in shrinkage, increased density, and reduced porosity, compromising biological function. When HDFs were seeded into 3 mg/mL tilapia fish collagen (F3), we observed scaffold contraction as expected, resulting in a condensed patch of cells at the side of the well at Day 6 (Figure S1).

To improve stability, we prepared composite scaffolds by blending various concentrations of fibrinogen with 3 mg/mL tilapia fish collagen. Fibrinogen was subsequently polymerized to form fibrin (Fbn) by thrombin addition in the media (Figure 3A). We observed that the composite scaffolds contracted in a concentration-dependent manner. After 14 days, only scaffolds blended with ≥ 0.5 mg/mL fibrin (F3-Fbn0.5, F3-Fbn1.0, F3-Fbn2.5 and F3-Fbn5.0) maintained their stable structure; in contrast, scaffolds with < 0.5 mg/mL fibrin content contracted into a condensed sphere, or partially contracted, pulling away from the edge of the well (Figure 3B).

In parallel, we examined the attachment of HEK cells to the apical surfaces of these collagen-fibrin scaffolds. Since keratinocytes do not express receptors for fibrinogen/fibrin, they are unable to attach to fibrin domains within the scaffold, leading to poor cell attachment and survival [59]. The survival of well-attached HEKs to different composite scaffolds was measured by the distribution of enzymatically reduced formazan particles, produced only by viable keratinocytes in the MTT assay. Two days after seeding HEKs, scaffolds with ≤ 0.5 mg/mL fibrin content (F3, F3-Fbn0.1 and F3-Fbn0.5) were able to support uniform keratinocyte attachment, indicated by the even formation of purple formazan particles over

scaffold surfaces. Conversely, scaffolds containing > 0.5 mg/mL fibrin showed a disrupted distribution of purple formazan particles (Figure S2). Keratinocytes were allowed to proliferate for an additional 2 days; however, the extended incubation only attenuated the patchy phenotype to a limited extent. Uneven keratinocyte attachment was still observed for F3-Fbn2.5 and F3-Fbn5.0 at Day 4, suggesting that higher fibrin concentrations in these composite scaffolds inhibited keratinocyte attachment and proliferation (Figure 3C).

To confirm that including a minimal amount of fibrin could improve the mechanical stability of fish collagen scaffolds, the rheological properties of F3 were compared to F3-Fbn0.5. Since mammalian collagens exhibit better mechanical stability [31], we used bovine collagen (B3) as comparison. While the polymerization times of F3 and B3 hydrogels were similar, B3 hydrogels exhibited higher storage modulus (G') and loss modulus (G'') than F3 hydrogels. For a viscoelastic material, the G' represents its ability to withstand deformation under load while the G'' determines its ability to accommodate rearrangements of its internal polymeric chains [60]. Addition of 0.5 mg/mL fibrin to generate F3-Fbn0.5 significantly increased the G' of fish collagen while the gelation time and G'' changed minimally (Table 1). Therefore, an increased G' correlates with enhanced resistance to mechanical deformation of the fully polymerized F3-Fbn0.5 hydrogels.

The optimized scaffold formulation of F3-Fbn0.5, henceforth indicated as fortified fish collagen (FFC) scaffold, was chosen for further characterization of cell compatibility, structural stability and ability to support the assembly of human skin tissue substitutes.

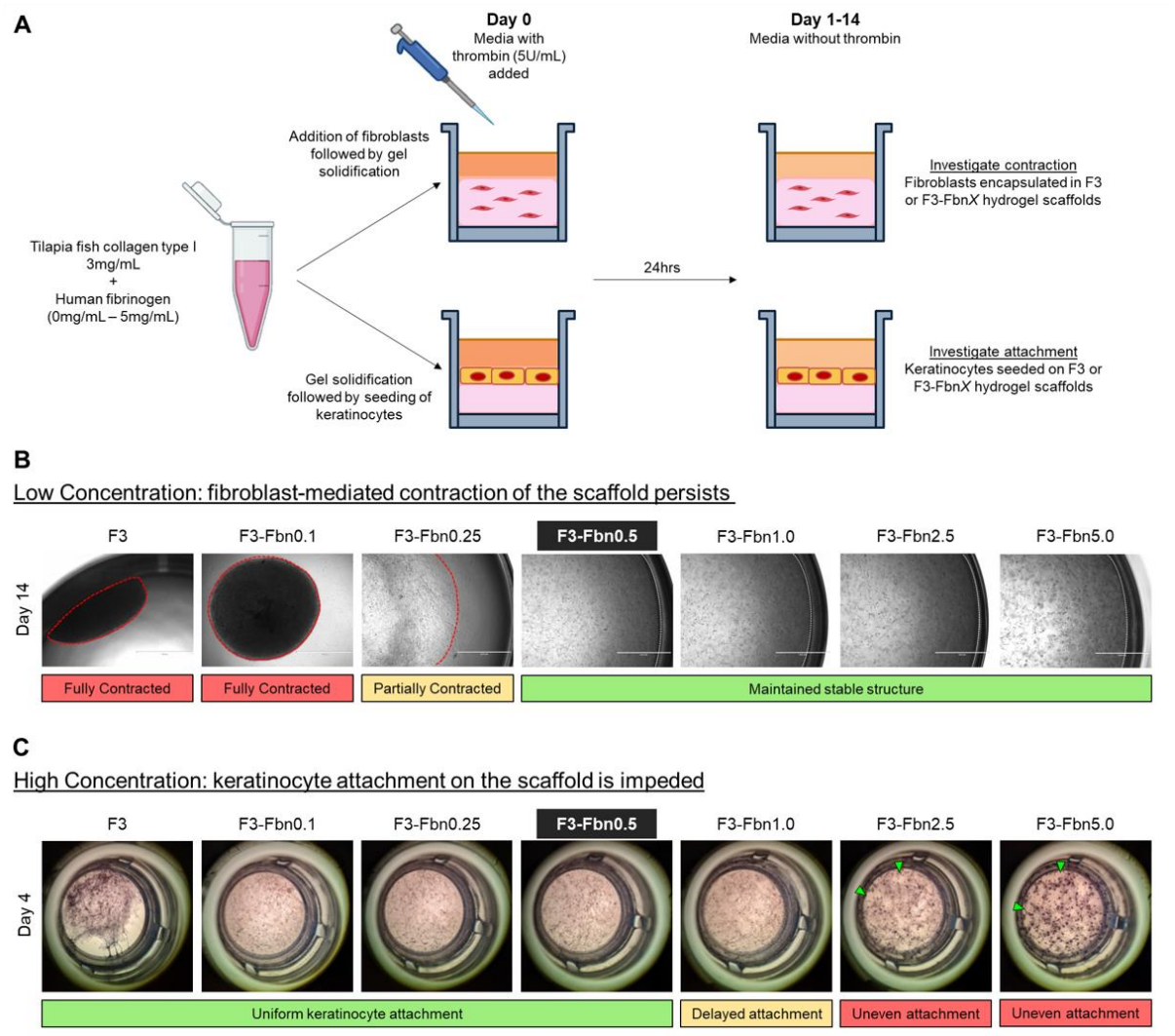

Figure 3. Optimization of fibrin concentration to minimize fibroblast-mediated contraction and improve keratinocyte attachment on collagen scaffolds. (A) Schematic illustrating the optimization process by mixing 3 mg/mL of fish collagen with variable concentrations of fibrinogen within the range of 0 mg/mL to 5 mg/mL. (F3 – fish collagen without fibrin; F3-Fbn*X* – fish collagen with fibrin, where *X* refers to the concentration of fibrin) (B) Fibroblast-mediated contraction of the collagen scaffold persisted at low concentrations of fibrin (0 mg/mL to 0.25 mg/mL), indicated by red dotted lines. Collagen scaffolds with 0.5 mg/mL to 5 mg/mL of fibrin (F3-Fbn0.5, F3-Fbn1.0, F3-Fbn2.5 and F3-Fbn5.0) maintained their initial size up to Day 14 and did not contract (indicated by white dotted lines). Scale bar = 1000 µm. (C) Keratinocyte attachment on the collagen scaffold is inhibited when fibrin concentrations are too high (2.5 mg/mL to 5 mg/mL), indicated by the discontinuous purple colouration (green arrows). Uniform attachment of keratinocytes was observed for collagen scaffolds with 0 mg/mL to 0.5 mg/mL of fibrin (F3, F3-Fbn0.1, F3-Fbn0.25 and F3-Fbn0.5).

Sample	Gel point (min) at 37˚C	G’ (Pa)	G’’ (Pa)
B3	18.2 ± 2.89	246 ± 26.3	31.4 ± 0.53
F3	15.2 ± 0.58	184 ± 8.1	14.6 ± 2.05
F3-Fbn0.5	14.1 ± 0.58	276 ± 28.4	19.3 ± 0.96

Storage modulus G' (G prime, in Pa); loss modulus G'' (G double prime, in Pa

Table 1. Rheological properties investigated for B3, F3 and F3-Fbn0.5.

3.3 Cell compatibility of fibrin fortified collagen scaffolds

To assess cell compatibility of optimized fortified fish collagen hydrogels, we investigated the viability, proliferation, and metabolism of HDFs cultivated in FFC constructs over a period of 14 days. For comparison, HDFs were also cultivated in fortified bovine collagen (FBC, B3-Fbn0.5 constructs) under identical conditions. Fibroblast viability was assayed at more than 85% in both FBC and FFC constructs (Figure 4A). Furthermore, the stacked confocal images recorded after different incubation periods revealed that the morphology of encapsulated fibroblasts progressed from spheroid to stellate geometry, suggesting that both FBC and FFC matrices support anchorage and spreading of HDFs (Figure 4B).

Fibroblast populations doubled after 14 days in culture for both scaffolds, with significant growth acceleration for fibroblasts embedded in FFC compared to FBC between day 4 and 11 (Figure 4C). This was further supported by the results from CellTiter-Glo® assays, which measure metabolic activity via ATP. The metabolic activity of fibroblasts cultured in FFC

scaffolds increased by 13-folds compared to the 10-fold increase in FBC counterparts (Figure 4D).

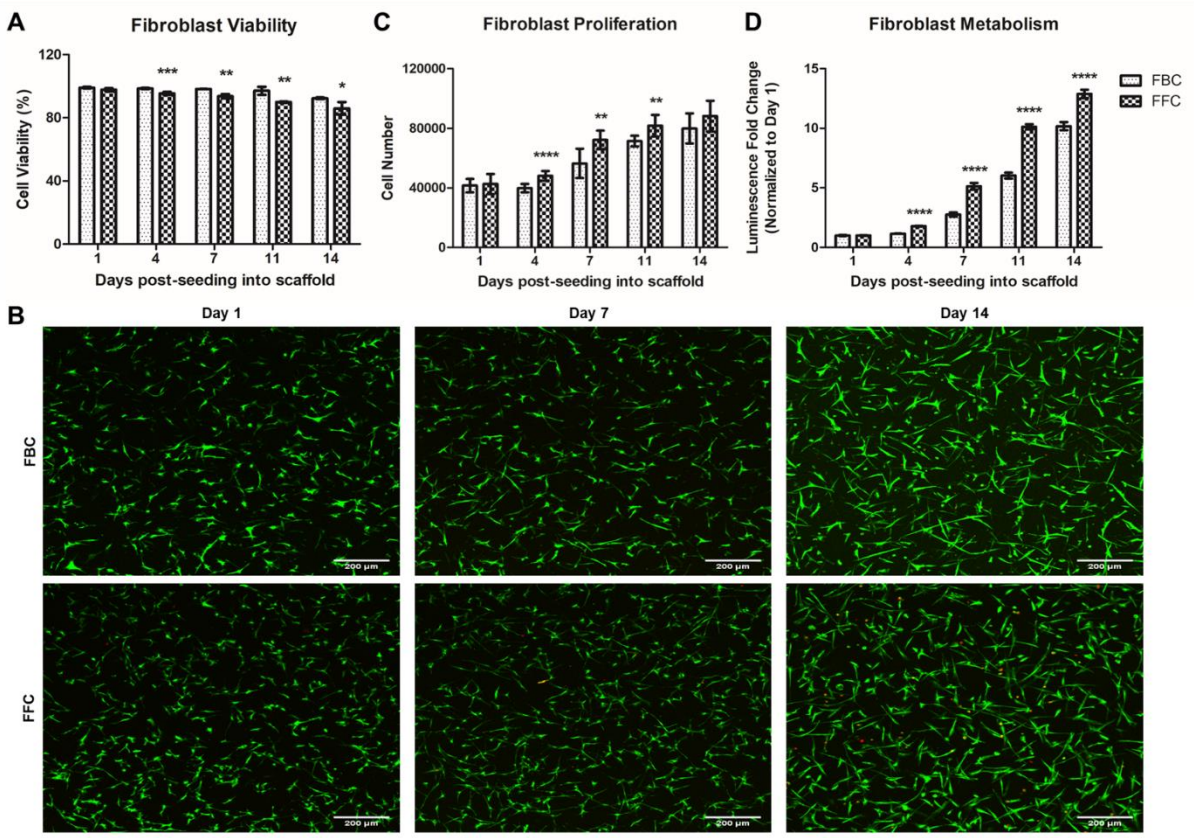

Figure 4. Cell compatibility of optimized F3-Fbn0.5 (i.e., fortified fish collagen (FFC)) scaffolds compared to mammalian collagen, B3-Fbn0.5 (i.e., fortified bovine collagen (FBC)). (A) Viability of fibroblasts encapsulated in FBC and FFC scaffolds determined using calcein-AM (Live) and ethidium homodimer (Dead) staining. (B) Stacked confocal images of the LIVE/DEAD assay over 14 days. Live cells fluoresce green, dead cells fluoresce red. Scale bar = 200 µm. (C) Proliferation of fibroblasts encapsulated FBC and FFC scaffolds determined by cell counting. (D) Metabolism of fibroblasts encapsulated in FBC and FFC scaffolds determined by CellTiter-Glo® Assay. Data indicate mean ± SD where * $p < 0.05$, ** $p < 0.01$, *** $p < 0.001$ and **** $p < 0.0001$ versus FBC (two-tailed unpaired t-tests); fibroblast viability (n = 4); fibroblast proliferation (n = 8); fibroblast metabolism (n = 4).

Overall, both FFC and FBC hydrogel scaffolds demonstrated good cell compatibility since fibroblast viability was well maintained while fibroblast numbers and metabolic activity increased in both scaffold types. The ability of FFC and FBC hydrogel scaffolds to support primary dermal fibroblasts may be attributed to intrinsic properties such as its capacity to present cell adhesion motifs, mechanical stability, as well as scaffold microarchitecture; in particular, porosity and pore size are known to influence cellular health [61]. Scanning electron microscopy (SEM) imaging of the acellular FBC and FFC scaffolds revealed a fibrous network of interconnected micropores, which can aid in efficient nutrient exchange and cell adhesion (Figure 5).

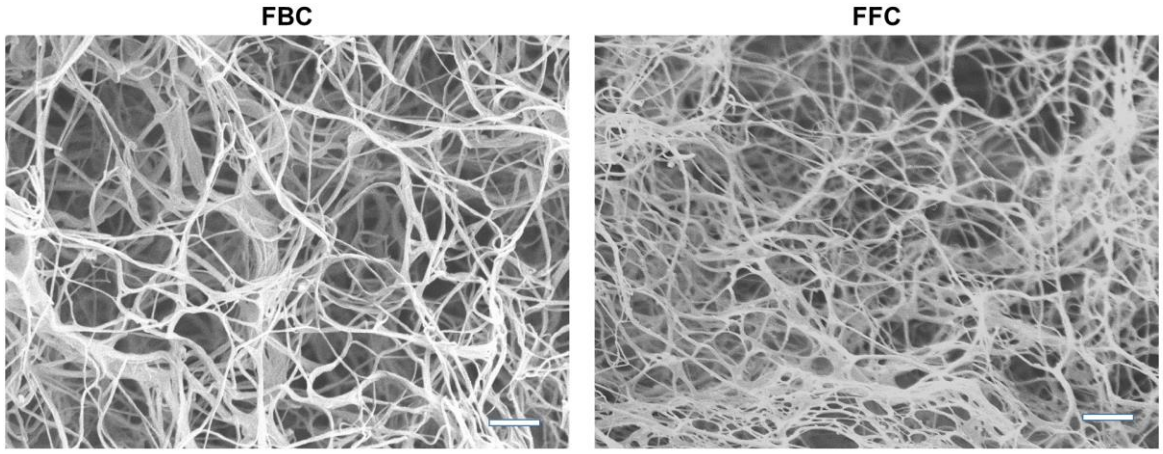

Figure 5. Scanning electron microscopy (SEM) imaging reveals FBC and FFC scaffolds are fibrous and highly porous. Scale bar = 1 µm

3.4 Stability of collagen-based human skin equivalents (HSEs) with or without fibrin fortification

To evaluate the capacity of FBC or FFC scaffolds to generate human skin equivalents (HSEs), we adopted a previously published protocol [62], detailed in Figure S3. During the airlift phase, contraction of the FBC and FFC HSEs were monitored via lateral (surface area) and vertical (height) measurements. At the same time, 3 mg/mL of bovine or fish collagen scaffolds without fibrin, were used to generate BC or FC HSEs as controls (Figure S4). Both BC and FC HSEs contracted, with FC HSEs contracting more compared to BC HSEs. This observation corresponds to the rheological data where F3 was found to have lower G', and thus lower mechanical strength, compared to B3.

Fortification of the scaffolds with fibrin greatly improved the stability of collagen-based HSEs, limiting lateral contraction i.e., reduction in surface area. HSEs generated using FBC, maintained 91.3 ± 10.5% of their original surface area (Figure 6A). In comparison, BC HSEs shrank to 44.4 ± 11.3% of their original area (Figure S4A). Improvements in lateral stability were even more prominent after blending fish collagen with fibrin; FFCs maintained their original circular shape and coverage of the Transwell® insert membrane throughout airlift incubation (Figure 6A). In contrast, FC HSEs contracted during airlift incubation, with 14.6 ± 8.6% of their original surface area remaining (Figure S4A). Although both collagen and collagen-fibrin HSEs exhibited vertical contraction, the inclusion of fibrin was found to minimize vertical shrinkage. As reported in Figure S4B, BC and FC HSEs shrank to less than 10% of their original height. Under identical conditions, FBC HSEs maintained 47.6 ± 9.2% of the original hydrogel height, and FFC HSEs maintained 63.3 ± 5.7 % of the original hydrogel height (Figure 6B).

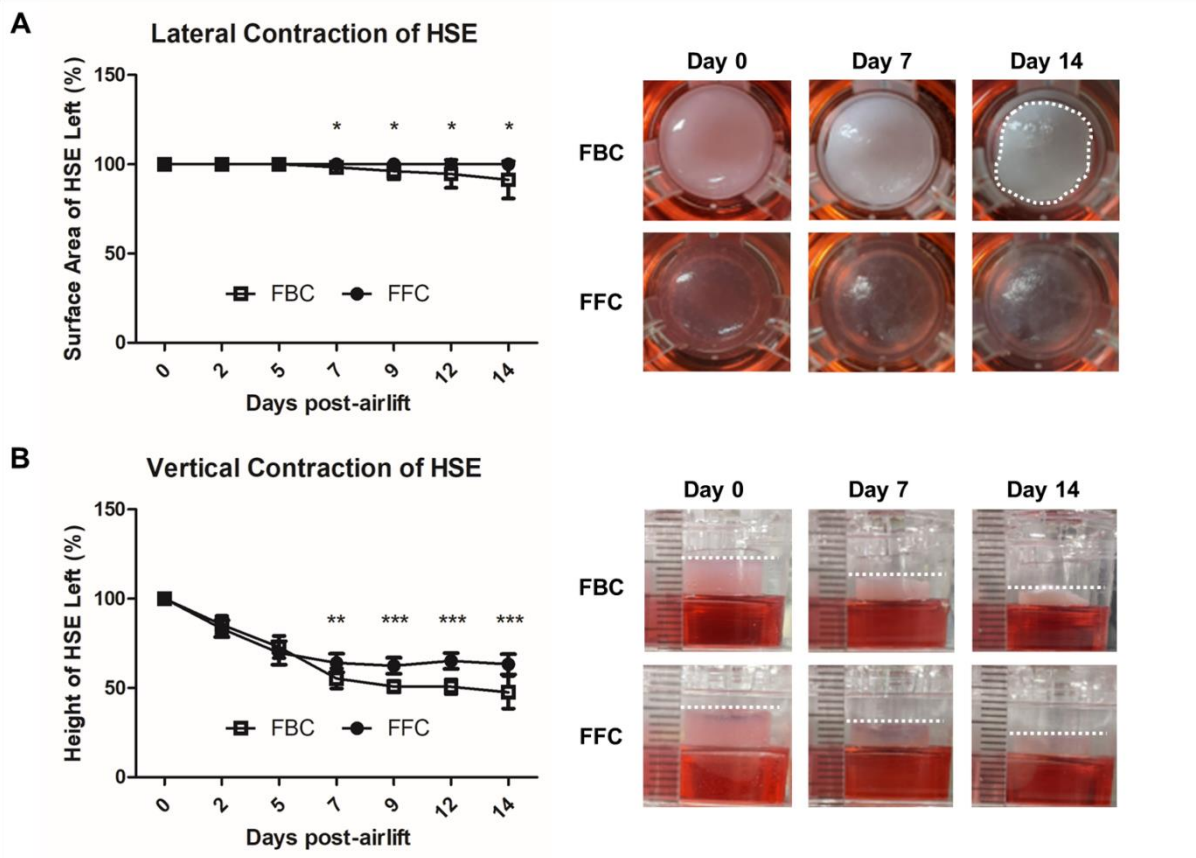

Figure 6. Fibrin fortification improved stability of fortified fish collagen (FFC) human skin equivalents (HSE) to a greater extent compared to fortified bovine collagen (FBC) HSEs. (A) FFC HSEs resisted lateral contraction even after 7 days incubation while FBC HSEs showed reduction in surface area (shrinkage of HSE surface area indicated by white dotted lines). (B) FFC HSEs exhibited a smaller decrease in scaffold height compared to FBC HSEs over 14 days of culture (height of HSEs indicated by white dotted lines). Data indicate mean ± SD where * $p < 0.05$, ** $p < 0.01$ and *** $p < 0.001$ versus FBC (two-tailed unpaired t-tests); FBC ($n = 6$); FFC ($n = 11$).

3.5 Structure and barrier function of FBC and FFC HSEs

Since the significant contractions of BC and FC HSEs gave rise to inconsistent *in vitro* models, we focused further structural investigations on the stable FBC and FFC HSEs. Histological and immunohistochemical (IHC) analyses of FBC and FFC HSEs were compared with MatTek's EpiDermFT™, a commercial full-thickness HSE model system, and with normal adult human skin (NHS).

We utilized classical hematoxylin and eosin (H&E) histology to visualize essential structural features of a mature epidermis: stratum basale, stratum spinosum, stratum granulosum and stratum corneum. Besides the absence of rete ridges, intact and fully-formed epidermis was observed to be attached to underlying dermal layers populated with fibroblasts in all skin models, comparable to NHS (Figure 7A).

To verify the cellular components of HSEs, we performed IHC to detect the expression and localization of characteristic epidermal markers in NHS, EpiDermFT™, FBC and FFC skin models (Figure 7B). In NHS, the intermediate filament protein Keratin 14 (K14), expressed by proliferating keratinocytes is localized to the basal layers of the epidermis. K14 expression is gradually lost as the keratinocytes differentiate and migrate apically into the suprabasal layers of the epidermis, where the expression of Keratin 10 (K10), is turned on starting from the stratum spinosum [63]. The distribution of K14 and K10 in EpiDermFT™ models was found to be similar to NHS. However, in FBC and FFC skin models, K14 was expressed in all skin layers; and, while restricted to suprabasal layers, the expression of K10 was sustained within higher layers of the epidermis. Loricrin, a major protein of the cornified cell envelope, is a marker for terminal epidermal differentiation in NHS and critical to barrier formation and maintenance of skin integrity [64]. Recapitulating human skin, we detected expression of

loricrin in the stratum granulosum of EpiDermFT™, FBC and FFC constructs. However, expression was found to be 'leaky' in some of the *in vitro* skin models, where weak expression was also observed in the stratum spinosum of EpiDermFT™ tissues and FBC HSEs.

Transmembrane proteins that mediate the inter-cellular adhesive functions of adherens junctions – E-cadherin [65], as well as regulate the inter-cellular permeability of tight junctions – Claudin I [66], are essential to establishing appropriate barrier function in mammalian skin. Mirroring their expression in NHS, the expression of E-cadherin and Claudin I was detected in all epidermal layers of the *in vitro* skin models that we tested. However, it was noted that the differential gradient expression of Claudin I in FFC constructs appeared to be more similar to the expression of Claudin I in NHS [67] compared to EpiDermFT™ and FBC constructs. Collagen IV is a significant protein secreted basally, contributing to the basement membrane at the boundary of epidermal and dermal tissues [68]. Collagen IV was found to be expressed and localized to epidermal-dermal junctions in all *in vitro* skin models.

Further, we investigated several characteristic nuclear species that contribute important regulatory functions to mammalian skin. The transcription factor p63 is an essential regulator of epithelial lineage commitment, proliferation, and differentiation. In human skin, the expression of p63 is found in proliferative keratinocytes of the lower epidermal layers [69]. We detected the expression and localization of p63 to be similar in NHS and all skin models. At the same time, we also probed for Ki67, a nuclear species that is only expressed by actively dividing cells. Measures of Ki67 provide the proliferation index, a percentage of actively dividing keratinocytes in the stratum basale of the epidermis. Measures of Ki67 reported by others indicate the proliferation index of NHS as 11.3 ± 2.1% [70,71]. For comparison, the

proliferation index measured for FBC HSEs was 9.4 ± 3.5%, and the proliferation index measured for FFC HSEs was 10.0 ± 2.3% (Figure S5).

The spatial distribution of fibroblasts in the dermal equivalent of each construct was also investigated using the mesenchymal cell marker Vimentin. Fibroblasts were observed to be uniformly distributed within the dermal equivalent matrix of all *in vitro* skin models. In contrast, the distribution of fibroblasts in our staining of NHS, as well as of those reported in literature, is concentrated in the papillary zone of the dermis while fewer fibroblasts are present in the reticular zone [72]. Predominantly, we found that while the FBC and FFC HSEs were structurally very similar to the commercially sourced EpiDermFT™, our fabricated HSEs exhibited small differences in expression and distribution of certain IHC markers. It is challenging to define which *in vitro* skin model was more representative of native human skin as each skin model had certain similarities and/or differences when compared to NHS.

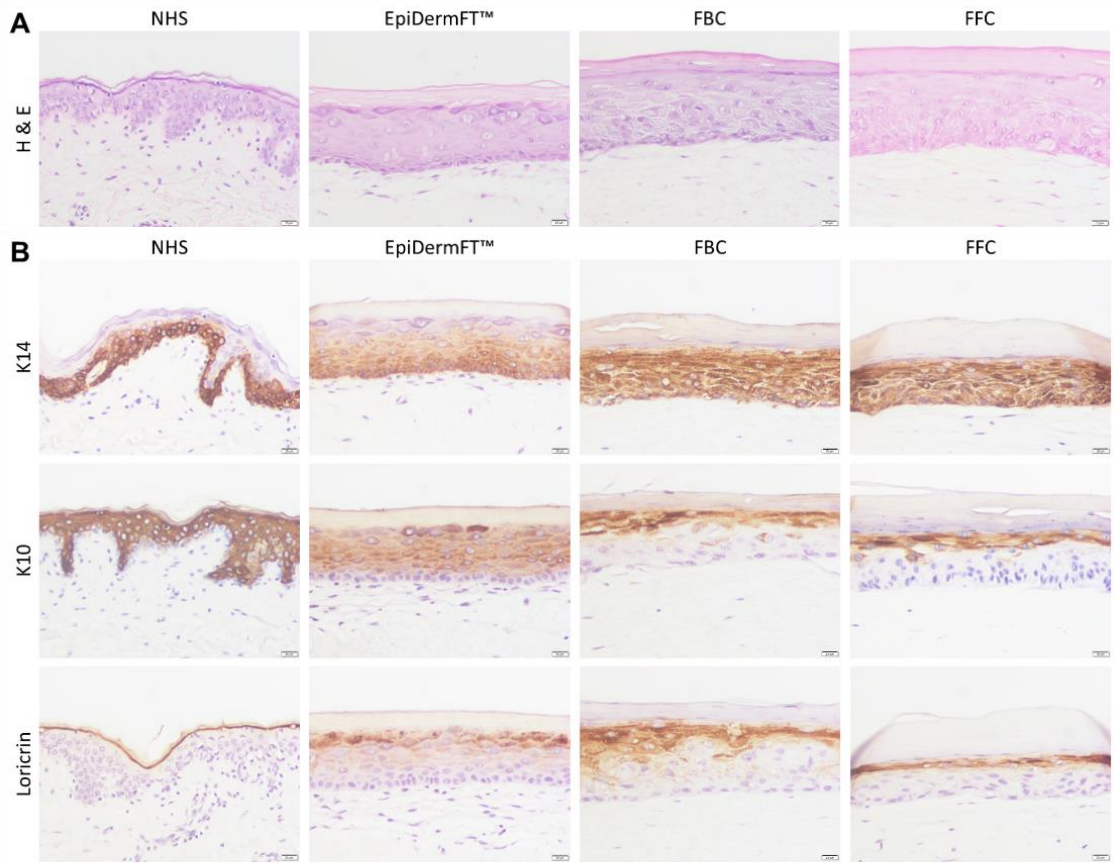

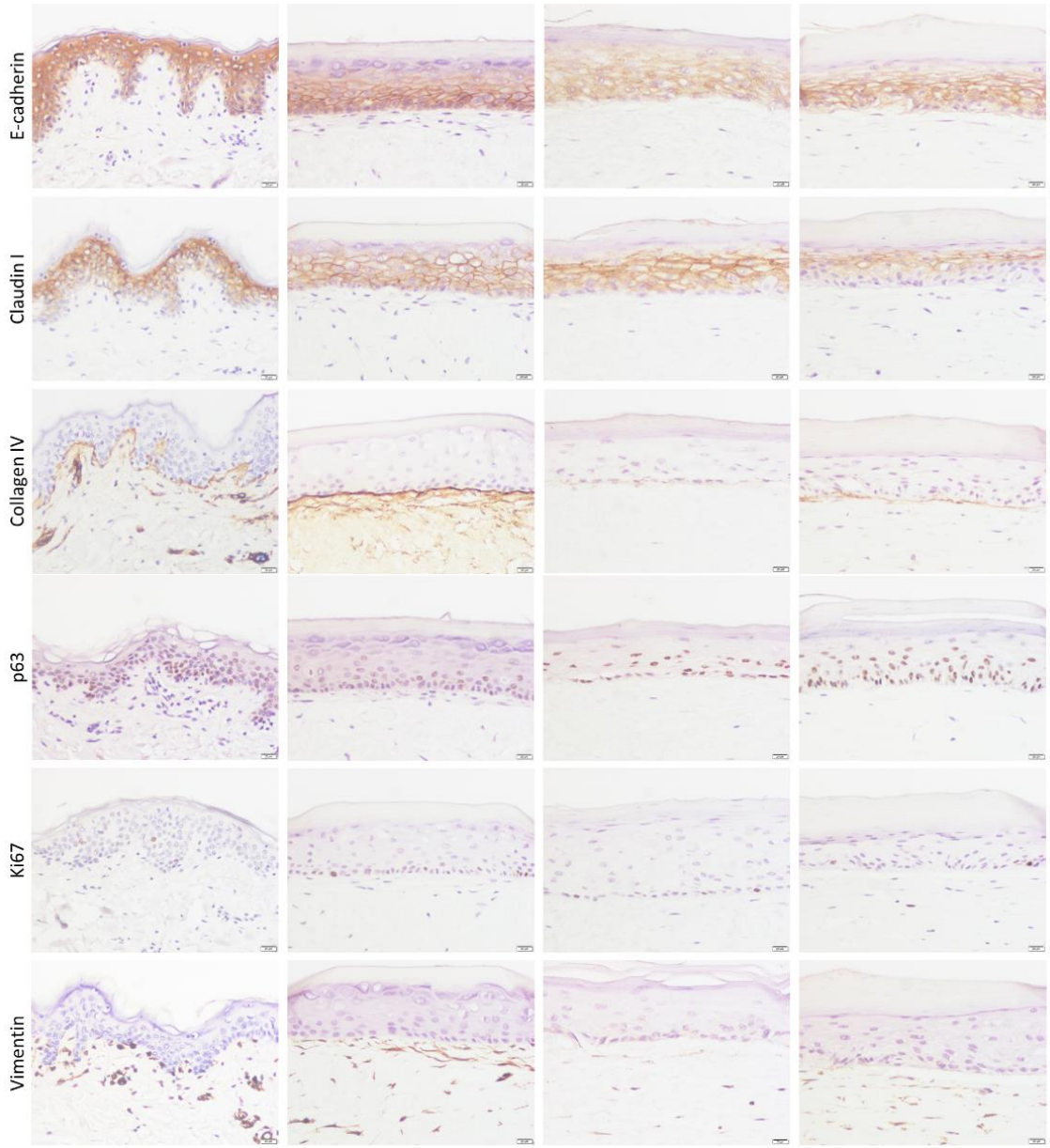

Figure 7. Histological and immunohistochemical analysis of normal human skin (NHS), EpiDermFT™, FBC and FFC HSEs (A) Hematoxylin and eosin staining (H&E) illustrates a stratified epidermis overlying fibroblast-populated dermis of NHS and the different *in vitro* skin models. (B) Immunohistochemical analysis was performed using antibodies specific for K14 (basal epidermis), K10 (early epidermal differentiation), Loricrin (late epidermal differentiation), E-cadherin (adherens junction protein), Claudin I (tight junction protein), Collagen IV (basement membrane protein), p63 and Ki67 (nuclear protein of proliferating cells), as well as Vimentin (fibroblast marker). Scale bar = 20 µm.

To validate the barrier function of the different skin models, we investigated the transepithelial electrical resistance (TEER) of EpiDermFT™, FBC and FFC HSEs. The TEER values of FFC HSEs were found to be significantly higher than both EpiDermFT™ and FBC skin models. We measured TEER values of 465.2 ± 54.6 Ωcm^2 for FFC constructs, more than 3 times higher than EpiDermFT™ (139.7 ± 63.8 Ωcm^2) and FBC HSEs (78.0 ± 29.7 Ωcm^2) (Figure 8).

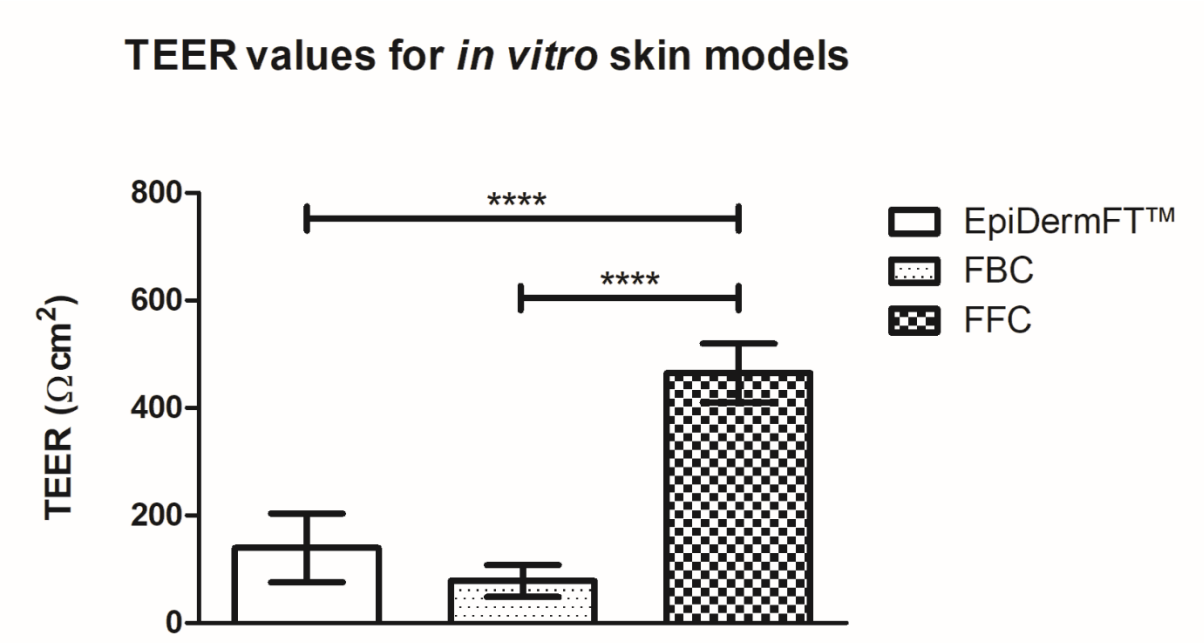

Figure 8. Measurement of transepithelial electrical resistance (TEER) of EpiDermFT™, FBC and FFC HSEs. Data indicate mean ± SD where **** $p < 0.0001$ (one-way ANOVA with Tukey's Multiple Comparison Test); EpiDermFT™ (n = 5); FBC (n = 9); FFC (n = 9).

3.6 96-well format FFC HSEs

The utility of *ex vivo* and *in vitro* human skin tissue models is limited by their amenity to mass production and ability to be adapted to existing high throughput screening platform technologies. To address this challenge, we explored scaling down the 12-well format HSEs used in this study, to fit in industry-standard 96-well plates. Compared to the 12 mm membrane diameter of 12-well Transwell® inserts, 96-well Transwell® inserts have a membrane diameter of 4.26 mm, providing a 10-fold reduction in reagents and cells required to fabricate the microscaled FFC (96-well FFC). Similar to FFC HSEs grown in the 12-well Transwell® inserts,

FFC HSEs grown in 96-well Transwell® inserts maintained their original surface area throughout the 14-day of air-liquid interface, although some vertical contraction was observed (Figure S6). At the end of the culture period, we observed the uniform distribution of purple formazan product over the hydrogel surface in MTT assay, indicating the formation of actively metabolizing and uniform epidermis.

4. Discussion

Collagens derived from marine species, especially fish, have recently attracted attention and recognition as potential substitutes for mammalian collagens, since they possess desirable properties such as low risk of zoonotic diseases, reduced antigenicity, good biocompatibility and high bioavailability [73]. Notably, collagen derived from tilapia, a fish species that usually inhabits shallow freshwater waterways, has already been evaluated for several applications such as bone, cartilage and skin tissue engineering [39,41,74], as well as drug delivery [75]. In the field of skin tissue engineering, these advantageous properties of tilapia-derived collagen make it an attractive biomaterial to assist the clinical management of cutaneous wounds. In addition, peptides derived from the Nile tilapia (*Oreochromis niloticus*) have been reported to exhibit antimicrobial properties [76] and support mammalian cell chemotaxis, aiding wound closure *in vitro* and *in vivo* [77,78]. Formulations prepared from other species of tilapia, have been claimed to promote the regrowth of hair [79]. Hence, tilapia fish collagen potentially presents an ideal biomaterial for *in vitro* skin reconstruction.

The increasing use of *in vitro* reconstructed tissue models, including human skin equivalent models, illustrates the transition that has occurred in recent years, replacing the use of traditional product testing systems (animal studies and human *ex vivo* skin) with human-equivalent, tissue-engineered reconstructed models [80]. Partly driven by the European Union's directive to prohibit the use of animals for product testing, the demand for appropriate, relevant, and accurate, human tissue equivalent technologies supports an emerging market for sustainable and low-cost type I collagens. In this work, we validated the potential of transforming post-consumer, discarded tilapia skin into high value type I collagen for health and medical applications. As proof-of-principle, we reformulated collagen scaffolds including collagens derived from tilapia fish skin, to fabricate *in vitro* 3D human skin models. As with

other collagen-based models, we found that strengthening of the collagen matrix was necessary. Fibrin, a natural biomaterial with established utility in reinforcing composite skin substitutes, was selected as a potential additive [44,46,81–83]. Blending fish collagen with an optimal amount of fibrin, resulted in a stable hydrogel scaffold, able to support fibroblast attachment and growth, forming a dermal equivalent, while simultaneously supporting keratinocyte attachment, proliferation, and differentiation, into a stratified epidermis.

Compared to other multicomponent collagen-fibrin formulations that utilize high concentrations of fibrinogen [46], our fortified fish collagen (FFC) formulation is much simpler, comprising of just two components: collagen blended with fibrin. A similar formulation, in which rat tail collagen (4 mg/mL) was blended with human fibrin (1 mg/mL), has been reported to generate HSEs [44]; although fibroblast-mediated contraction of their *in vitro* skin construct was observed. While superficially similar, we argue that the results reported for this study are not comparable with our FFC formulated HSEs due to multiple differences such as collagen source, number of cells seeded and variations in medium components [44]. In our evaluation, HSEs constructed using FFC demonstrated superior stability over HSEs constructed with FC, BC, and FBC, maintaining their original surface area and exhibiting minimal vertical compression over the 14-day incubation period at the air-liquid interface. Resistance to contraction is important for downstream applications since consistent tissue morphology is critical to ensure accuracy and reproducibility when assaying tissue responses to topically applied compounds, and measures of skin barrier function, such as TEER.

A robust and stable dermal template is essential to support authentic development and maturation of full-thickness human skin. We critically evaluated the anatomical features of FFC and FBC skin models, using the commercially sourced EpiDermFT™ (MatTek) skin

model and native human skin for comparison. FFC and FBC skin equivalents were found to be anatomically equivalent to the validated EpiDermFT™ skin model, with minor differences in the level of expression and distribution of certain molecular markers. Notably, the expression of K14 was detected in all epidermal layers of FFC and FBC constructs, whereas K14 was restricted to the basal compartment in EpiDermFT™ constructs and native human skin. This atypical distribution of K14 may possibly be due to the ethnicity of tissue donors of dermal fibroblasts since donor ethnicity has been reported to affect K14 expression and epidermal differentiation processes in reconstructed human skin [84]. Our cell donors were from Asian origin. To confirm whether the atypical K14 expression affected differentiation in the FFC and FBC skin models, we examined the expression of K10 and Loricrin, proteins expressed during early and late phases of epidermal differentiation respectively. Our analysis confirmed that both K10 and Loricrin were expressed in suprabasal layers of FFC and FBC skin models. The role of donor ethnicity in FFC and FBC HSEs will be further investigated in future studies. Regardless of the slight differences we detected, each of the skin models we constructed *in vitro* were determined to be physiologically similar to native human skin.

Considering the practical applications for FFC and FBC HSEs, we analyzed barrier function parameters of FFC and FBC HSEs and compared these measures with those acquired from EpiDermFT™. Transepithelial electrical resistance (TEER) is a well-established, non-invasive assay for assessing barrier integrity and permeability, where intact, stratified epidermis generally results in a higher TEER measure [85,86]. Interestingly, TEER values from EpiDermFT™ were 3 times lower than those recorded from FFC skin constructs. TEER values recorded from FFC constructs were also observed to be much higher than values recorded from FBC constructs. We postulate that this could be due to current leakage in sample replicates where the dermis, or epidermis, were not well attached to the walls of the Transwell® insert.

It has been reported that a less than 99.6% tissue coverage over the culture area can lead to an 80% reduction in TEER values [87]. Another possible explanation for the low TEER measures we observed in FBC HSEs, is suboptimal basement membrane formation. This hypothesis was supported by the weak staining of Collagen IV in FBC HSEs. Proper formation of the basement membrane, assembly of tight junctions, and lipid composition of the stratum corneum all make significant contributions to epidermal barrier integrity [88–90].

Fabricating HSEs in formats that are compatible with high throughput / high content analyses is a priority for industrial applications. With this in mind, we evaluated the potential impact of scaling down the FFC HSE constructs, from 12-well Transwell® platform to the industry-standard 96-well high throughput platform. Adopting the 96-well Transwell® format for FFC skin constructs (96-well FFC) reduced raw materials use by 10-fold, and coincidently reduced the consumption of limited donor tissues, cells and reagents. We demonstrated that 96-well FFCs were able to maintain their surface area throughout the 14-day duration of cultivation at the air-liquid interface. While some vertical contraction was observed, constructs remained metabolically active and viable; demonstrated by MTT staining. While we manually prepared 96-well FFCs in this proof-of-principle study, we suggest that emerging liquid-handling technologies, for example, bioprinting, will deliver efficiencies, reduce inter-well variation thereby improving reliability, reproducibility, and minimizing assay variance.

5. Conclusion

Valorization of what is currently by-product waste of fishing industries has transformed low value discarded tilapia skin, into high value-add, disease-free and hypoallergenic collagen suitable for diverse health and medical applications. The method we applied to harvest collagens from tilapia fish skin is cost-effective, yields high purity product, and can be

produced from sustainable resources. Through fibrin fortification, we have expanded the utility of fish-derived collagen in *in vitro* skin reconstruction to demonstrate proof-of-principle. The resulting product, fortified fish collagen (FFC), is formulated for human cell compatibility, mechanical strength and resistance to cell-mediated contraction. In this study, we have shown that stable 3D *in vitro* skin models can be constructed using FFC scaffolds. Notwithstanding, the FFC HSE platform possesses substantial potential for applications in pre-clinical evaluations of dermatological compounds such as toxicity testing, skin permeation and penetration studies as well as sensitivity testing. We demonstrated that when grown in a 12-well format, the FFC skin constructs are accessible to industry-standard TEER methodologies for the rapid assessment of skin barrier integrity. We further demonstrated that the FFC skin constructs can be scaled down to grow in 96-well format, further expanding its utility and application for high throughput applications.

CRediT authorship contribution statement

Shi Hua Tan: Conceptualization, Investigation, Formal analysis, Project administration, Visualization, Writing - original draft. **Shaoqiong Liu:** Investigation, Writing - review & editing. **Swee Hin Teoh:** Resources, Writing - review & editing. **Carine Bonnard:** Resources, Writing - review & editing. **David Leavesley:** Resources, Writing - review & editing. **Kun Liang:** Conceptualization, Investigation, Funding acquisition, Resources, Supervision, Writing - review & editing.

Conflict of interest statement

The authors declare no conflicts of interest.

Acknowledgements

We would like to thank the Asian Skin Biobank at the Skin Research Institute of Singapore (SRIS) for providing primary dermal fibroblasts and epidermal keratinocytes. This research is supported by the Agency for Science, Technology and Research (A*STAR) RIE2020 Advanced Manufacturing and Engineering (AME) programmatic grant (A18A8b0059) Additive Manufacturing for Biological Materials (AMBM) project, A*STAR IAF-PP (H1701a0004) The Skin Research Institute of Singapore, Phase 2: SRIS@Novena and A*STAR CDF < C210112030>.

Appendix A. Supplementary Data

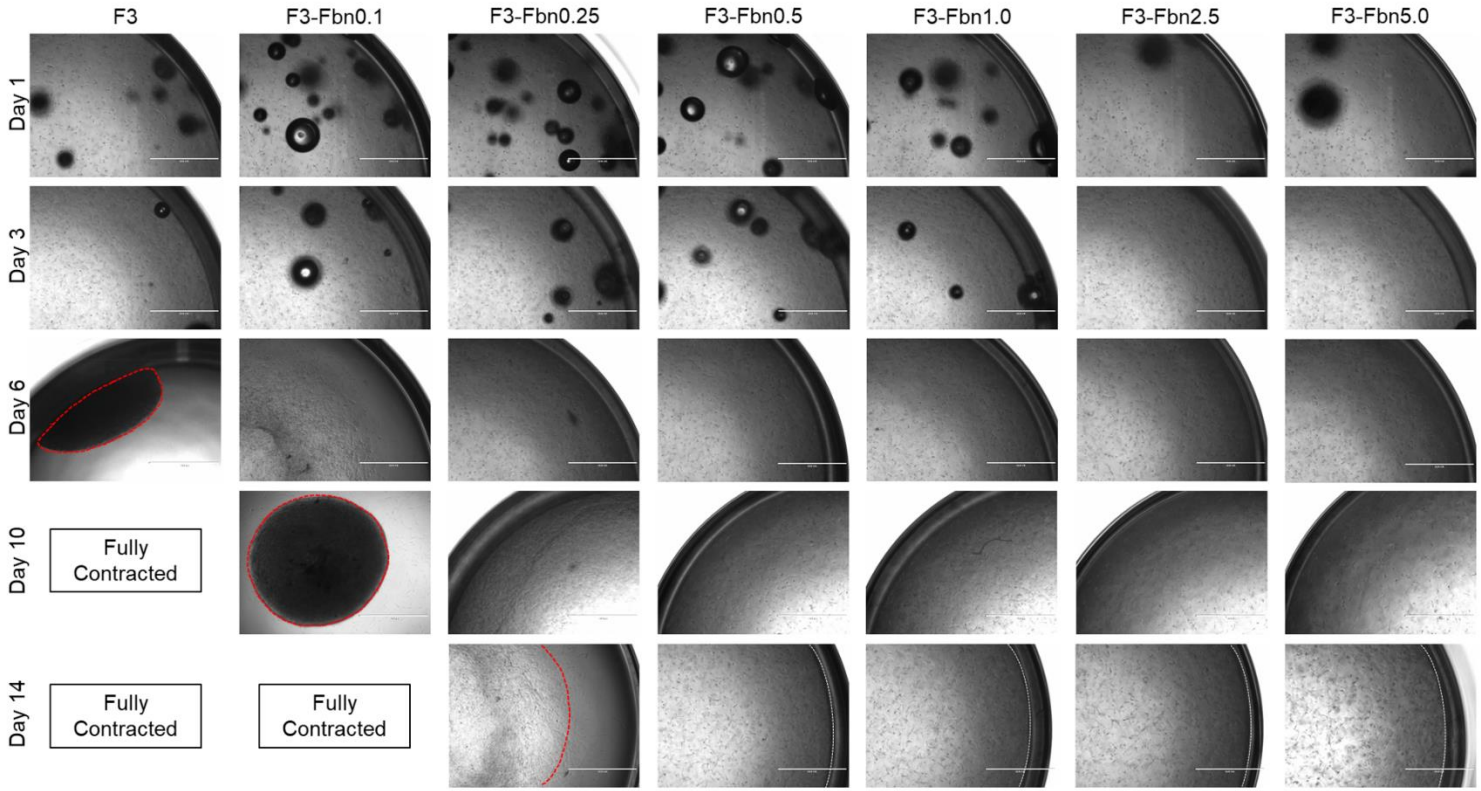

Figure S1. The concentration of fibrin was optimized to address the issue of contraction in fibroblast-encapsulated collagen scaffolds. 3 mg/mL of fish collagen was mixed with variable concentrations of fibrin (Fbn) from 0 mg/mL (F3) to 5 mg/mL (F3-Fbn5.0). F3 hydrogel scaffolds were the first to contract, forming a condensed patch of cells at the side of the well at Day 6. F3-Fbn0.1 were the next to contract at Day 10, followed by F3-Fbn0.25, which showed signs of contraction at Day 14. Hydrogel scaffolds with 0.5 mg/mL to 5 mg/mL of fibrin (F3-Fbn0.5, F3-Fbn1.0, F3-Fbn2.5 and F3-Fbn5.0) maintained their initial sizes up to Day 14 and did not shrink. Contracted scaffold boundaries are indicated by red dotted lines while uncontracted scaffolds are indicated by white dotted lines. Scale bar = 1000 µm.

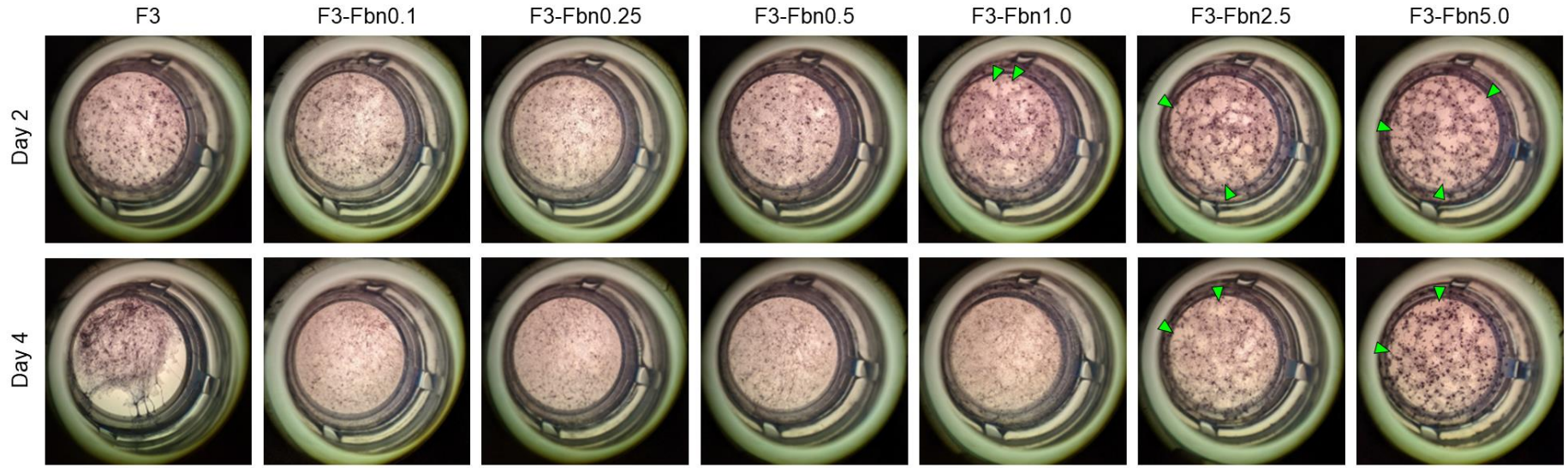

Figure S2. The concentration of fibrin was investigated to ensure proper keratinocyte attachment and viability on collagen-fibrin hydrogel scaffolds. 3 mg/mL of fish collagen was mixed with variable concentrations of fibrin (Fbn) from 0 mg/mL (F3) to 5 mg/mL (F3-Fbn5.0). Well-attached keratinocytes were metabolically active and converted MTT to insoluble formazan, turning the surface of the hydrogel purple. At Day 2 post-seeding, scaffolds with 1 mg/mL to 5 mg/mL fibrin (F3-Fbn1.0, F3-Fbn2.5 and F3-Fbn5.0) showed uneven keratinocyte attachment, indicated by the patchy purple coloration and large gaps with no cells (green arrows). Keratinocytes were allowed to proliferate for an additional 2 days however, the increase in keratinocyte numbers attenuated the patchy phenotype to a limited extent as uneven keratinocyte attachment was still observed for F3-Fbn2.5 and F3-Fbn5.0 at Day 4, suggesting that fibrin concentrations were too high for keratinocytes to attach and proliferate.

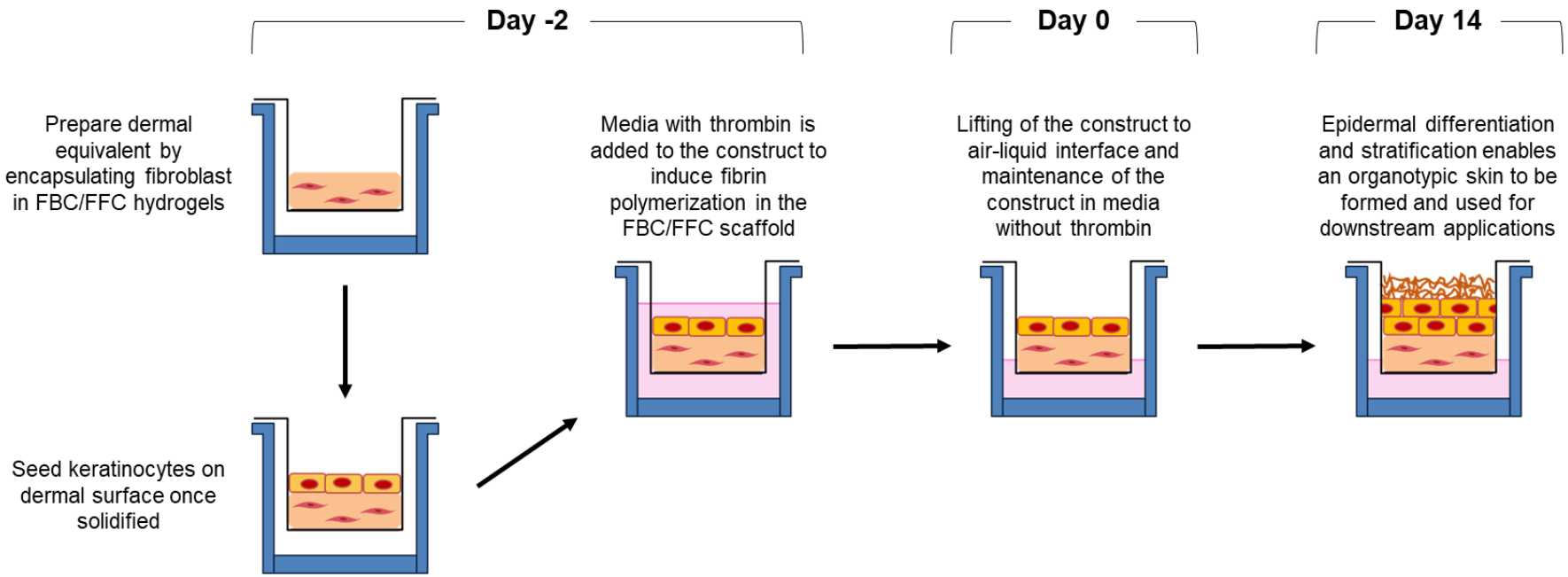

Figure S3. Fabrication process of the organotypic skin model based on FBC or FFC as the dermal equivalent. Fibroblast-encapsulated FBC/FFC hydrogels were solidified in Transwell® inserts followed by seeding of keratinocytes on the dermal surface. The co-culture construct was maintained submerged in media for 2 days, after which it was lifted to air-liquid interface, and cultured for another 14 days, inducing epidermal differentiation and stratification.

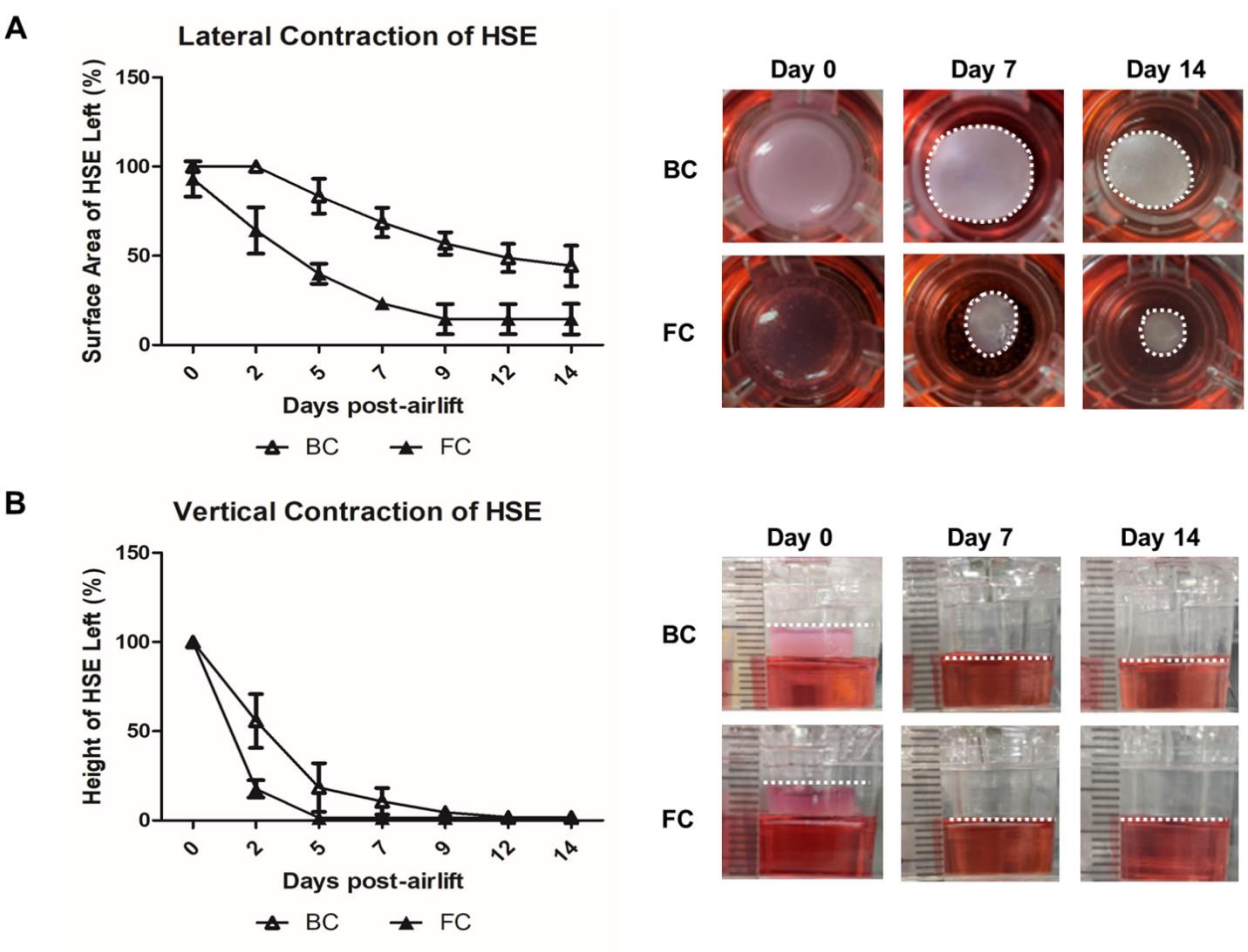

Figure S4. Bovine collagen (BC) and fish collagen (FC) human skin equivalents (HSEs) without fibrin fortification underwent severe lateral and vertical contraction. (A) BC HSEs started to shrink laterally (i.e., reduction in surface area) from Day 2 onwards while FC HSEs underwent a dramatic reduction in surface area immediately after airlifting (shrinkage of HSE surface area indicated by white dotted lines). (B) BC and FC HSEs underwent severe vertical contraction (i.e., decreased height), indicated by white dotted lines. Data indicate mean ± SD; BC (n = 5); FC (n = 2).

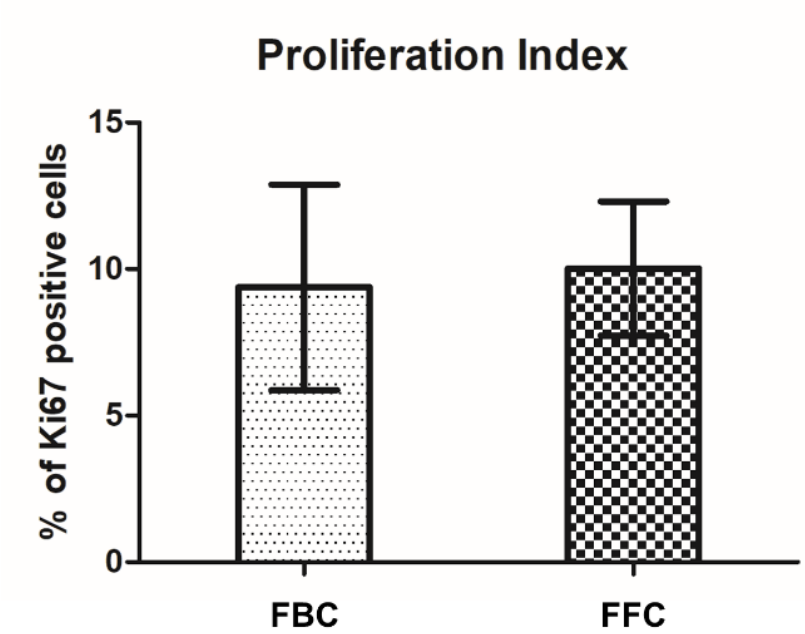

Figure S5. Proliferation index of FBC and FFC skin models. The percentage of Ki67 positive cells found in FBC HSEs was 9.4 ± 3.5 % (n = 3) while FFC HSEs was 10.0 ± 2.3% (n = 5).

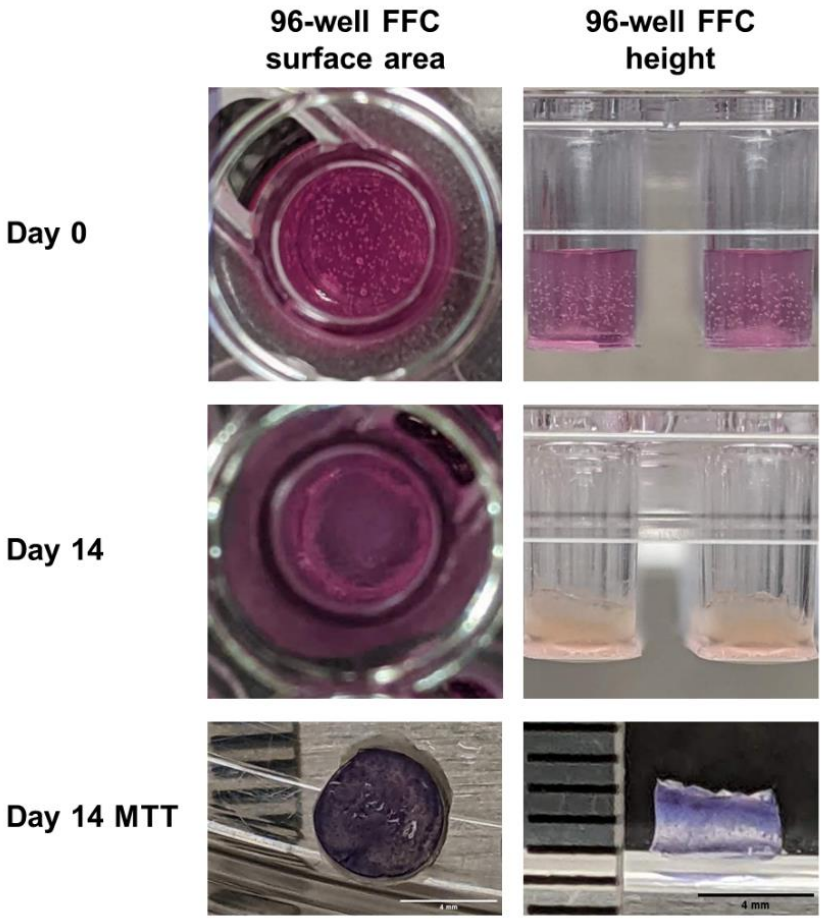

Figure S6. Scaling down of FFC HSEs cultured in 96-well Transwell® formats (96-well FFC). 96-well FFC HSEs maintained their surface area throughout the entire culture period while some vertical contraction was observed. The even distribution of purple formazan precipitate from the metabolized MTT reagent, over the HSE surface indicates the presence of a uniform, intact, and live epidermis. Scale bar = 4 mm.

References

[1] E. Abd, S. Yousuf, M. Pastore, K. Telaprolu, Y. Mohammed, S. Namjoshi, J. Grice, M. Roberts, Skin models for the testing of transdermal drugs, Clin. Pharmacol. Adv. Appl. Volume 8 (2016) 163–176. https://doi.org/10.2147/CPAA.S64788.

[2] P. Avci, M. Sadasivam, A. Gupta, W.C. De Melo, Y.-Y. Huang, R. Yin, R. Chandran, R. Kumar, A. Otufowora, T. Nyame, M.R. Hamblin, Animal models of skin disease for drug discovery, Expert Opin. Drug Discov. 8 (2013) 331–355. https://doi.org/10.1517/17460441.2013.761202.

[3] P.B. Medawar, The Cultivation of Adult Mammalian Skin Epithelium In Vitro, J. Cell Sci. s3-89 (1948) 187–196. https://doi.org/10.1242/jcs.s3-89.6.187.

[4] DIRECTIVE 2010/63/EU OF THE EUROPEAN PARLIAMENT AND OF THE COUNCIL of 22 September 2010 on the protection of animals used for scientific purposes, THE EUROPEAN PARLIAMENT, 2010.

[5] J.R. Yu, J. Navarro, J.C. Coburn, B. Mahadik, J. Molnar, J.H. Holmes, A.J. Nam, J.P. Fisher, Current and Future Perspectives on Skin Tissue Engineering: Key Features of Biomedical Research, Translational Assessment, and Clinical Application, Adv. Healthc. Mater. 8 (2019) 1801471. https://doi.org/10.1002/ADHM.201801471.

[6] I.N. Amirrah, Y. Lokanathan, I. Zulkiflee, M.F.M.R. Wee, A. Motta, M.B. Fauzi, A Comprehensive Review on Collagen Type I Development of Biomaterials for Tissue Engineering: From Biosynthesis to Bioscaffold, Biomedicines. 10 (2022) 2307. https://doi.org/10.3390/biomedicines10092307.

[7] L. Gu, T. Shan, Y. Ma, F.R. Tay, L. Niu, Novel Biomedical Applications of Crosslinked Collagen, Trends Biotechnol. 37 (2019) 464–491. https://doi.org/10.1016/j.tibtech.2018.10.007.

[8] B.S. Kim, J.-S. Lee, G. Gao, D.-W. Cho, Direct 3D cell-printing of human skin with

functional transwell system, Biofabrication. 9 (2017) 025034. https://doi.org/10.1088/1758-5090/aa71c8.

[9] Q. Muller, M.-J. Beaudet, T. De Serres-Bérard, S. Bellenfant, V. Flacher, F. Berthod, Development of an innervated tissue-engineered skin with human sensory neurons and Schwann cells differentiated from iPS cells, Acta Biomater. 82 (2018) 93–101. https://doi.org/10.1016/j.actbio.2018.10.011.

[10] E. Bellas, M. Seiberg, J. Garlick, D.L. Kaplan, In vitro 3D Full-Thickness Skin-Equivalent Tissue Model Using Silk and Collagen Biomaterials, Macromol. Biosci. 12 (2012) 1627–1636. https://doi.org/10.1002/mabi.201200262.

[11] C. Lotz, F.F. Schmid, E. Oechsle, M.G. Monaghan, H. Walles, F. Groeber-Becker, Cross-linked Collagen Hydrogel Matrix Resisting Contraction To Facilitate Full-Thickness Skin Equivalents, ACS Appl. Mater. Interfaces. 9 (2017) 20417–20425. https://doi.org/10.1021/acsami.7b04017.

[12] H.E. Abaci, Z. Guo, A. Coffman, B. Gillette, W. Lee, S.K. Sia, A.M. Christiano, Human Skin Constructs with Spatially Controlled Vasculature Using Primary and iPSC- Derived Endothelial Cells, Adv. Healthc. Mater. 5 (2016) 1800–1807. https://doi.org/10.1002/adhm.201500936.

[13] J. Zimoch, D. Zielinska, K. Michalak-Micka, D. Rütsche, R. Böni, T. Biedermann, A.S. Klar, Bio-engineering a prevascularized human tri-layered skin substitute containing a hypodermis, Acta Biomater. 134 (2021) 215–227. https://doi.org/10.1016/j.actbio.2021.07.033.

[14] K. Kim, S. Jeong, G.Y. Sung, Effect of Periodical Tensile Stimulation on the Human Skin Equivalents by Magnetic Stretching Skin-on-a-Chip (MSSC), BioChip J. 16 (2022) 501–514. https://doi.org/10.1007/s13206-022-00092-x.

[15] K. Kim, H. Kim, G.Y. Sung, An Interleukin-4 and Interleukin-13 Induced Atopic

Dermatitis Human Skin Equivalent Model by a Skin-On-A-Chip, Int. J. Mol. Sci. 23 (2022) 2116. https://doi.org/10.3390/ijms23042116.

[16] Z. Rajabimashhadi, N. Gallo, L. Salvatore, F. Lionetto, Collagen Derived from Fish Industry Waste: Progresses and Challenges, Polymers (Basel). 15 (2023) 544. https://doi.org/10.3390/polym15030544.

[17] F. Subhan, M. Ikram, A. Shehzad, A. Ghafoor, Marine Collagen: An Emerging Player in Biomedical applications, J. Food Sci. Technol. 52 (2015) 4703–4707. https://doi.org/10.1007/s13197-014-1652-8.

[18] S. Liu, C.S. Lau, K. Liang, F. Wen, S.H. Teoh, Marine collagen scaffolds in tissue engineering, Curr. Opin. Biotechnol. 74 (2022) 92–103. https://doi.org/10.1016/j.copbio.2021.10.011.

[19] L. Salvatore, N. Gallo, M.L. Natali, L. Campa, P. Lunetti, M. Madaghiele, F.S. Blasi, A. Corallo, L. Capobianco, A. Sannino, Marine collagen and its derivatives: Versatile and sustainable bio-resources for healthcare, Mater. Sci. Eng. C. 113 (2020) 110963. https://doi.org/10.1016/j.msec.2020.110963.

[20] Y.-S. Lim, Y.-J. Ok, S.-Y. Hwang, J.-Y. Kwak, S. Yoon, Marine Collagen as A Promising Biomaterial for Biomedical Applications, Mar. Drugs. 17 (2019) 467. https://doi.org/10.3390/md17080467.

[21] N. Xu, X.-L. Peng, H.-R. Li, J.-X. Liu, J.-S.-Y. Cheng, X.-Y. Qi, S.-J. Ye, H.-L. Gong, X.-H. Zhao, J. Yu, G. Xu, D.-X. Wei, Marine-Derived Collagen as Biomaterials for Human Health, Front. Nutr. 8 (2021) 493. https://doi.org/10.3389/fnut.2021.702108.

[22] H. Jafari, A. Lista, M.M. Siekapen, P. Ghaffari-Bohlouli, L. Nie, H. Alimoradi, A. Shavandi, Fish collagen: Extraction, characterization, and applications for biomaterials engineering, Polymers (Basel). 12 (2020) 1–37. https://doi.org/10.3390/polym12102230.

[23] M. Blanco, J. Vázquez, R. Pérez-Martín, C. Sotelo, Hydrolysates of Fish Skin Collagen: An Opportunity for Valorizing Fish Industry Byproducts, Mar. Drugs. 15 (2017) 131. https://doi.org/10.3390/md15050131.

[24] D. Liu, G. Wei, T. Li, J. Hu, N. Lu, J.M. Regenstein, P. Zhou, Effects of alkaline pretreatments and acid extraction conditions on the acid-soluble collagen from grass carp (Ctenopharyngodon idella) skin, Food Chem. 172 (2015) 836–843. https://doi.org/10.1016/j.foodchem.2014.09.147.

[25] D. Coppola, M. Oliviero, G.A. Vitale, C. Lauritano, I. D'Ambra, S. Iannace, D. de Pascale, Marine Collagen from Alternative and Sustainable Sources: Extraction, Processing and Applications, Mar. Drugs. 18 (2020) 214. https://doi.org/10.3390/md18040214.

[26] C.G. Sotelo, M.B. Comesaña, P.R. Ariza, R.I. Pérez-Martín, Characterization of Collagen from Different Discarded Fish Species of the West Coast of the Iberian Peninsula, J. Aquat. Food Prod. Technol. 25 (2016) 388–399. https://doi.org/10.1080/10498850.2013.865283.

[27] R.J. Mullins, H. James, T.A.E. Platts-Mills, S. Commins, Relationship between red meat allergy and sensitization to gelatin and galactose-α-1,3-galactose, J. Allergy Clin. Immunol. 129 (2012) 1334-1342.e1. https://doi.org/10.1016/j.jaci.2012.02.038.

[28] J.W. Steinke, T.A.E. Platts-Mills, S.P. Commins, The alpha-gal story: Lessons learned from connecting the dots, J. Allergy Clin. Immunol. 135 (2015) 589–596. https://doi.org/10.1016/j.jaci.2014.12.1947.

[29] M. Akita, Y. Nishikawa, Y. Shigenobu, D. Ambe, T. Morita, K. Morioka, K. Adachi, Correlation of proline, hydroxyproline and serine content, denaturation temperature and circular dichroism analysis of type I collagen with the physiological temperature of marine teleosts, Food Chem. 329 (2020) 126775.

https://doi.org/10.1016/j.foodchem.2020.126775.

[30] Z. Bao, Y. Sun, K. Rai, X. Peng, S. Wang, R. Nian, M. Xian, The promising indicators of the thermal and mechanical properties of collagen from bass and tilapia: synergistic effects of hydroxyproline and cysteine, Biomater. Sci. 6 (2018) 3042–3052. https://doi.org/10.1039/C8BM00675J.

[31] H. Ahn, D.J. Gong, H.H. Lee, J.Y. Seo, K.-M. Song, S.J. Eom, S.Y. Yeo, Mechanical Properties of Porcine and Fish Skin-Based Collagen and Conjugated Collagen Fibers, Polymers (Basel). 13 (2021) 2151. https://doi.org/10.3390/polym13132151.

[32] J. Li, M. Wang, Y. Qiao, Y. Tian, J. Liu, S. Qin, W. Wu, Extraction and characterization of type I collagen from skin of tilapia (Oreochromis niloticus) and its potential application in biomedical scaffold material for tissue engineering, Process Biochem. 74 (2018) 156–163. https://doi.org/10.1016/j.procbio.2018.07.009.

[33] W.K. Song, D. Liu, L.L. Sun, B.F. Li, H. Hou, Physicochemical and Biocompatibility Properties of Type I Collagen from the Skin of Nile Tilapia (Oreochromis niloticus) for Biomedical Applications, Mar. Drugs. 17 (2019). https://doi.org/10.3390/md17030137.

[34] S. Zeng, C. Zhang, H. Lin, P. Yang, P. Hong, Z. Jiang, Isolation and characterisation of acid-solubilised collagen from the skin of Nile tilapia (Oreochromis niloticus), Food Chem. 116 (2009) 879–883. https://doi.org/10.1016/j.foodchem.2009.03.038.

[35] N.M. Zain, S. Saidin, A. Sosiawan, Properties of Tilapia Collagen as a Biomaterial for Tissue Engineering: A Review, IOP Conf. Ser. Mater. Sci. Eng. 932 (2020) 012021. https://doi.org/10.1088/1757-899X/932/1/012021.

[36] J.M. Munguti, R. Nairuti, J.O. Iteba, K.O. Obiero, D. Kyule, M.A. Opiyo, J. Abwao, J.G. Kirimi, N. Outa, M. Muthoka, C.M. Githukia, E.O. Ogello, Nile tilapia (Oreochromis niloticus Linnaeus, 1758) culture in Kenya: Emerging production

technologies and socio- economic impacts on local livelihoods, Aquac. Fish Fish. 2 (2022) 265–276. https://doi.org/10.1002/aff2.58.

[37] L. Sun, B. Li, D. Yao, W. Song, H. Hou, Effects of cross-linking on mechanical, biological properties and biodegradation behavior of Nile tilapia skin collagen sponge as a biomedical material, J. Mech. Behav. Biomed. Mater. 80 (2018) 51–58. https://doi.org/10.1016/j.jmbbm.2018.01.006.

[38] Y. Zhuang, S. Ruan, H. Yao, Y. Sun, Physical Properties of Composite Films from Tilapia Skin Collagen with Pachyrhizus Starch and Rambutan Peel Phenolics, Mar. Drugs. 17 (2019) 662. https://doi.org/10.3390/md17120662.

[39] A.M. Hassanbhai, C.S. Lau, F. Wen, P. Jayaraman, B.T. Goh, N. Yu, S.-H. Teoh, In Vivo Immune Responses of Cross-Linked Electrospun Tilapia Collagen Membrane, Tissue Eng. Part A. 23 (2017) 1110–1119. https://doi.org/10.1089/ten.tea.2016.0504.

[40] S. Yao, Y. Shang, B. Ren, S. Deng, Z. Wang, Y. Peng, Z. Huang, S. Ma, C. Peng, S. Hou, A novel natural-derived tilapia skin collagen mineralized with hydroxyapatite as a potential bone-grafting scaffold, J. Biomater. Appl. 37 (2022) 219–237. https://doi.org/10.1177/08853282221086246.

[41] H. Li, R. Chen, Z. Jia, C. Wang, Y. Xu, C. Li, H. Xia, D. Meng, Porous fish collagen for cartilage tissue engineering., Am. J. Transl. Res. 12 (2020) 6107–6121. /pmc/articles/PMC7653596/.

[42] T. Zhou, B. Sui, X. Mo, J. Sun, Multifunctional and biomimetic fish collagen/bioactive glass nanofibers: fabrication, antibacterial activity and inducing skin regeneration in vitro and in vivo, Int. J. Nanomedicine. Volume 12 (2017) 3495–3507. https://doi.org/10.2147/IJN.S132459.

[43] Y.-D. Nien, Y.-P. Han, B. Tawil, L.S. Chan, T.-L. Tuan, W.L. Garner, Fibrinogen inhibits fibroblast-mediated contraction of collagen, Wound Repair Regen. 11 (2003)

380–385. https://doi.org/10.1046/j.1524-475X.2003.11511.x.

[44] A. Malheiro, M. Thon, A.F. Lourenço, A.S. Gamardo, A. Chandrakar, S. Gibbs, P. Wieringa, L. Moroni, A Humanized In Vitro Model of Innervated Skin for Transdermal Analgesic Testing, Macromol. Biosci. 23 (2023) 2200387. https://doi.org/10.1002/mabi.202200387.

[45] N. Hakimi, R. Cheng, L. Leng, M. Sotoudehfar, P.Q. Ba, N. Bakhtyar, S. Amini-Nik, M.G. Jeschke, A. Günther, Handheld skin printer: in situ formation of planar biomaterials and tissues, Lab Chip. 18 (2018) 1440–1451. https://doi.org/10.1039/C7LC01236E.

[46] K. Derr, J. Zou, K. Luo, M.J. Song, G.S. Sittampalam, C. Zhou, S. Michael, M. Ferrer, P. Derr, Fully Three-Dimensional Bioprinted Skin Equivalent Constructs with Validated Morphology and Barrier Function, Tissue Eng. Part C Methods. 25 (2019) 334–343. https://doi.org/10.1089/ten.tec.2018.0318.

[47] M. Albanna, K.W. Binder, S. V. Murphy, J. Kim, S.A. Qasem, W. Zhao, J. Tan, I.B. El-Amin, D.D. Dice, J. Marco, J. Green, T. Xu, A. Skardal, J.H. Holmes, J.D. Jackson, A. Atala, J.J. Yoo, In Situ Bioprinting of Autologous Skin Cells Accelerates Wound Healing of Extensive Excisional Full-Thickness Wounds, Sci. Rep. 9 (2019) 1856. https://doi.org/10.1038/s41598-018-38366-w.

[48] C.M. Brougham, T.J. Levingstone, S. Jockenhoevel, T.C. Flanagan, F.J. O'Brien, Incorporation of fibrin into a collagen–glycosaminoglycan matrix results in a scaffold with improved mechanical properties and enhanced capacity to resist cell-mediated contraction, Acta Biomater. 26 (2015) 205–214. https://doi.org/10.1016/j.actbio.2015.08.022.

[49] S. Liu, F. Wen, P. Muthukumaran, M. Rakshit, C.-S. Lau, N. Yu, L. Suryani, Y. Dong, S.H. Teoh, Self-Assembled Nanofibrous Marine Collagen Matrix Accelerates Healing

of Full-Thickness Wounds, ACS Appl. Bio Mater. 4 (2021) 7044–7058. https://doi.org/10.1021/acsabm.1c00685.

[50] S.Q. Liu, Q. Tian, J.L. Hedrick, J.H. Po Hui, P.L. Rachel Ee, Y.Y. Yang, Biomimetic hydrogels for chondrogenic differentiation of human mesenchymal stem cells to neocartilage, Biomaterials. 31 (2010) 7298–7307. https://doi.org/10.1016/j.biomaterials.2010.06.001.

[51] H. Green, K. Easley, S. Iuchi, Marker succession during the development of keratinocytes from cultured human embryonic stem cells, Proc. Natl. Acad. Sci. 100 (2003) 15625–15630. https://doi.org/10.1073/pnas.0307226100.

[52] M. Simon, H. Green, Enzymatic cross-linking of involucrin and other proteins by keratinocyte particulates in vitro, Cell. 40 (1985) 677–683. https://doi.org/10.1016/0092-8674(85)90216-8.

[53] J.G. Rheinwald, H. Green, Serial cultivation of strains of human epidermal keratinocytes: the formation keratinizing colonies from single cells, Cell. 6 (1975) 331–343. https://doi.org/10.1016/S0092-8674(75)80001-8.

[54] Z. Rastian, S. Pütz, Y. Wang, S. Kumar, F. Fleissner, T. Weidner, S.H. Parekh, Type I Collagen from Jellyfish Catostylus mosaicus for Biomaterial Applications, ACS Biomater. Sci. Eng. 4 (2018) 2115–2125. https://doi.org/10.1021/acsbiomaterials.7b00979.

[55] D. Fassini, I.C. Wilkie, M. Pozzolini, C. Ferrario, M. Sugni, M.S. Rocha, M. Giovine, F. Bonasoro, T.H. Silva, R.L. Reis, Diverse and Productive Source of Biopolymer Inspiration: Marine Collagens, Biomacromolecules. 22 (2021) 1815–1834. https://doi.org/10.1021/acs.biomac.1c00013.

[56] Y. Feng, G. Melacini, J.P. Taulane, M. Goodman, Acetyl-Terminated and Template-Assembled Collagen-Based Polypeptides Composed of Gly-Pro-Hyp Sequences. 2.

Synthesis and Conformational Analysis by Circular Dichroism, Ultraviolet Absorbance, and Optical Rotation, J. Am. Chem. Soc. 118 (1996) 10351–10358. https://doi.org/10.1021/ja961260c.

[57] J.E.M. Souren, M. Ponec, R. Wijk, Contraction of collagen by human fibroblasts and keratinocytes, Vitr. Cell. Dev. Biol. 25 (1989) 1039–1045. https://doi.org/10.1007/BF02624138.

[58] F. Grinnell, Fibroblast–collagen-matrix contraction: growth-factor signalling and mechanical loading, Trends Cell Biol. 10 (2000) 362–365. https://doi.org/10.1016/S0962-8924(00)01802-X.

[59] M. Kubo, L. Van De Water, L.C. Plantefaber, M.W. Mosesson, M. Simon, M.G. Tonnesen, L. Taichman, R.A.F. Clark, Fibrinogen and Fibrin are Anti-Adhesive for Keratinocytes: A Mechanism for Fibrin Eschar Slough During Wound Repair, J. Invest. Dermatol. 117 (2001) 1369–1381. https://doi.org/10.1046/j.0022-202x.2001.01551.x.

[60] S.H. Tan, D.A.C. Chua, J.R.J. Tang, C. Bonnard, D. Leavesley, K. Liang, Design of hydrogel-based scaffolds for in vitro three-dimensional human skin model reconstruction, Acta Biomater. 153 (2022) 13–37. https://doi.org/10.1016/j.actbio.2022.09.068.

[61] B.P. Chan, K.W. Leong, Scaffolding in tissue engineering: general approaches and tissue-specific considerations, Eur. Spine J. 17 (2008) 467–479. https://doi.org/10.1007/s00586-008-0745-3.

[62] C. Arnette, J.L. Koetsier, P. Hoover, S. Getsios, K.J. Green, In Vitro Model of the Epidermis, in: Methods Enzymol., 2016: pp. 287–308. https://doi.org/10.1016/bs.mie.2015.07.015.

[63] F. Wang, A. Zieman, P.A. Coulombe, Skin Keratins, in: Int. J. Mol. Sci. 2020, Vol. 21,

Page 2271, Multidisciplinary Digital Publishing Institute, 2016: pp. 303–350. https://doi.org/10.1016/bs.mie.2015.09.032.

[64] Y. Ishitsuka, D.R. Roop, Loricrin: Past, Present, and Future, Int. J. Mol. Sci. 21 (2020) 2271. https://doi.org/10.3390/ijms21072271.

[65] F. Furukawa, K. Fujii, Y. Horiguchi, N. Matsuyoshi, M. Fujita, K.-I. Toda, S. Imamura, H. Wakita, S. Shirahama, M. Takigawa, Roles of E- and P-cadherin in the human skin, Microsc. Res. Tech. 38 (1997) 343–352. https://doi.org/10.1002/(SICI)1097-0029(19970815)38:4<343::AID-JEMT2>3.0.CO;2-K.

[66] A. Hartsock, W.J. Nelson, Adherens and tight junctions: Structure, function and connections to the actin cytoskeleton, Biochim. Biophys. Acta - Biomembr. 1778 (2008) 660–669. https://doi.org/10.1016/j.bbamem.2007.07.012.

[67] S. Bergmann, B. von Buenau, S. Vidal-y-Sy, M. Haftek, E. Wladykowski, P. Houdek, S. Lezius, H. Duplan, K. Bäsler, S. Dähnhardt-Pfeiffer, C. Gorzelanny, S.W. Schneider, E. Rodriguez, D. Stölzl, S. Weidinger, J.M. Brandner, Claudin-1 decrease impacts epidermal barrier function in atopic dermatitis lesions dose-dependently, Sci. Rep. 10 (2020) 2024. https://doi.org/10.1038/s41598-020-58718-9.

[68] A. Abreu-Velez, M. Howard, Collagen IV in normal skin and in pathological processes, N. Am. J. Med. Sci. 4 (2012) 1. https://doi.org/10.4103/1947-2714.92892.

[69] V.A. Botchkarev, E.R. Flores, p53/p63/p73 in the Epidermis in Health and Disease, Cold Spring Harb. Perspect. Med. 4 (2014) a015248–a015248. https://doi.org/10.1101/cshperspect.a015248.

[70] S. Gibbs, A.N. Silva Pinto, S. Murli, M. Huber, D. Hohl, M. Ponec, Epidermal growth factor and keratinocyte growth factor differentially regulate epidermal migration, growth, and differentiation, Wound Repair Regen. 8 (2000) 192–203.

https://doi.org/10.1046/j.1524-475x.2000.00192.x.

[71] A. Mieremet, A. Vázquez García, W. Boiten, R. van Dijk, G. Gooris, J.A. Bouwstra, A. El Ghalbzouri, Human skin equivalents cultured under hypoxia display enhanced epidermal morphogenesis and lipid barrier formation, Sci. Rep. 9 (2019) 7811. https://doi.org/10.1038/s41598-019-44204-4.

[72] J.M. Sorrell, A.I. Caplan, Fibroblast heterogeneity: more than skin deep, J. Cell Sci. 117 (2004) 667–675. https://doi.org/10.1242/jcs.01005.

[73] M. Furtado, L. Chen, Z. Chen, A. Chen, W. Cui, Development of fish collagen in tissue regeneration and drug delivery, Eng. Regen. 3 (2022) 217–231. https://doi.org/10.1016/j.engreg.2022.05.002.

[74] B. Ge, H. Wang, J. Li, H. Liu, Y. Yin, N. Zhang, S. Qin, Comprehensive Assessment of Nile Tilapia Skin (Oreochromis niloticus) Collagen Hydrogels for Wound Dressings, Mar. Drugs. 18 (2020) 178. https://doi.org/10.3390/md18040178.

[75] M.M. Anwar, M.A. Shalaby, H. Saeed, H.M. Mostafa, D.G. Hamouda, H. Nounou, Theophylline-encapsulated Nile Tilapia fish scale-based collagen nanoparticles effectively target the lungs of male Sprague–Dawley rats, Sci. Rep. 12 (2022) 4871. https://doi.org/10.1038/s41598-022-08880-z.

[76] H.-N. Huang, Y.-L. Chan, C.-J. Wu, J.-Y. Chen, Tilapia Piscidin 4 (TP4) Stimulates Cell Proliferation and Wound Closure in MRSA-Infected Wounds in Mice, Mar. Drugs. 13 (2015) 2813–2833. https://doi.org/10.3390/md13052813.

[77] Z.I. Elbialy, A. Atiba, A. Abdelnaby, I.I. Al-Hawary, A. Elsheshtawy, H.A. El-Serehy, M.M. Abdel-Daim, S.E. Fadl, D.H. Assar, Collagen extract obtained from Nile tilapia (Oreochromis niloticus L.) skin accelerates wound healing in rat model via up regulating VEGF, bFGF, and α-SMA genes expression, BMC Vet. Res. 16 (2020) 352. https://doi.org/10.1186/s12917-020-02566-2.

[78] Z. Hu, P. Yang, C. Zhou, S. Li, P. Hong, Marine Collagen Peptides from the Skin of Nile Tilapia (Oreochromis niloticus): Characterization and Wound Healing Evaluation, Mar. Drugs. 15 (2017) 102. https://doi.org/10.3390/md15040102.

[79] S. Bin Hwang, H.J. Park, B.-H. Lee, Hair-Growth-Promoting Effects of the Fish Collagen Peptide in Human Dermal Papilla Cells and C57BL/6 Mice Modulating Wnt/β-Catenin and BMP Signaling Pathways, Int. J. Mol. Sci. 23 (2022) 11904. https://doi.org/10.3390/ijms231911904.

[80] F.A. Auger, F. Berthod, V.´ Eronique Moulin, R. Pouliot, L. Germain, Tissue-engineered skin substitutes: from in vitro constructs to in vivo applications, Biotechnol. Appl. Biochem. 39 (2004) 263–275. https://doi.org/10.1042/BA20030229.

[81] M.I. Quiñones-Vico, A. Fernández-González, E. Pérez-Castejón, T. Montero-Vílchez, S. Arias-Santiago, Cytotoxicity and Epidermal Barrier Function Evaluation of Common Antiseptics for Clinical Use in an Artificial Autologous Skin Model, J. Clin. Med. 10 (2021) 642. https://doi.org/10.3390/jcm10040642.

[82] A. Montero, C. Atienza, C. Elvira, J.L. Jorcano, D. Velasco, Hyaluronic acid-fibrin hydrogels show improved mechanical stability in dermo-epidermal skin substitutes, Mater. Sci. Eng. C. 128 (2021) 112352. https://doi.org/10.1016/j.msec.2021.112352.

[83] M. Sheikholeslam, M.E.E. Wright, M.G. Jeschke, S. Amini-Nik, Biomaterials for Skin Substitutes, Adv. Healthc. Mater. 7 (2018) 1700897. https://doi.org/10.1002/adhm.201700897.

[84] S. Girardeau-Hubert, C. Deneuville, H. Pageon, K. Abed, C. Tacheau, N. Cavusoglu, M. Donovan, D. Bernard, D. Asselineau, Reconstructed Skin Models Revealed Unexpected Differences in Epidermal African and Caucasian Skin, Sci. Rep. 9 (2019) 7456. https://doi.org/10.1038/s41598-019-43128-3.

[85] B. Srinivasan, A.R. Kolli, M.B. Esch, H.E. Abaci, M.L. Shuler, J.J. Hickman, TEER

Measurement Techniques for In Vitro Barrier Model Systems, SLAS Technol. 20 (2015) 107–126. https://doi.org/10.1177/2211068214561025.

[86] P. Zoio, S. Ventura, M. Leite, A. Oliva, Pigmented Full-Thickness Human Skin Model Based on a Fibroblast-Derived Matrix for Long-Term Studies, Tissue Eng. Part C Methods. 27 (2021) 433–443. https://doi.org/10.1089/ten.tec.2021.0069.

[87] M. Odijk, A.D. van der Meer, D. Levner, H.J. Kim, M.W. van der Helm, L.I. Segerink, J.-P. Frimat, G.A. Hamilton, D.E. Ingber, A. van den Berg, Measuring direct current trans-epithelial electrical resistance in organ-on-a-chip microsystems, Lab Chip. 15 (2015) 745–752. https://doi.org/10.1039/C4LC01219D.

[88] K.C. Madison, Barrier Function of the Skin: "La Raison d'Être" of the Epidermis, J. Invest. Dermatol. 121 (2003) 231–241. https://doi.org/10.1046/j.1523-1747.2003.12359.x.

[89] D. Breitkreutz, I. Koxholt, K. Thiemann, R. Nischt, Skin Basement Membrane: The Foundation of Epidermal Integrity—BM Functions and Diverse Roles of Bridging Molecules Nidogen and Perlecan, Biomed Res. Int. 2013 (2013) 1–16. https://doi.org/10.1155/2013/179784.

[90] M. Yokouchi, A. Kubo, Maintenance of tight junction barrier integrity in cell turnover and skin diseases, Exp. Dermatol. 27 (2018) 876–883. https://doi.org/10.1111/exd.13742.